2011-12-16

Influence of Weak Interactions on Supramolecular Binding: Characterization of Cucurbituril Complexes with Alkylmonoammonium Ions Using Fourier Transform Ion Cyclotron Resonance Mass Spectrometry

Ruijan Shi
Brigham Young University - Provo

Influence of Weak Interactions on Supramolecular Binding: Characterization of Cucurbituril Complexes with Alkylmonoammonium Ions Using Fourier Transform Ion Cyclotron Resonance Mass Spectrometry

Ruijun Shi

A thesis submitted to the faculty of
Brigham Young University
In partial fulfillment of the requirements for the degree of

Master of Science

David V. Dearden, Chair
John D. Lamb
Daniel E. Austin

Department of Chemistry and Biochemistry

Brigham Young University

December 2011

ABSTRACT

Influence of Weak Interactions on Supramolecular Binding: Characterization of Cucurbituril Complexes with Alkylmonoammonium Ions Using Fourier Transform Ion Cyclotron Resonance Mass Spectrometry

Ruijun Shi
Department of Chemistry and Biochemistry
Master of Science

This thesis focuses on using mass spectrometry-based techniques for characterizing the structure and behavior of cucurbituril complexes in the gas phase. Both solvent and counter ion effects can be completely eliminated in the gas phase and the intrinsic interactions in the system are directly shown in the experimental results.

Chapter 1 introduces the structures, properties and host-guest chemistry of cucurbituril, and FTICR mass spectrometry including instrumentation, performance and working principles. Two mass spectrometry-based methods for supramolecular characterization, sustained off-resonance irradiation collision induced dissociation (SORI CID) and ion molecule equilibrium measurements, are also discussed in this chapter.

Chapter 2 characterizes the dissociation and reaction behaviors of the complexes formed by cucurbit[5]uril (CB5) and primary monoamines [$CH_3(CH_2)_nNH_2$, n = 0-7] as well as similar studies of decamethylcucurbit[5]uril (mc5) in the gas phase. This study probes host-guest interactions between the neutral cucurbituril host and alkyl chains of varying length. All the cucurbit[5]uril and decamethylcucurbit[5]uril complexes have external binding. The dissociation thresholds of the complexes suggest that the optimum monoammonium chain length for binding CB5 in the gas phase occurs for n = 2, whereas for mc5 the optimum is n = 0. Reactivity studies of CB5 and mc5 complexes indicate the highest binding affinity appears at n = 6 for CB5 and n = 5 for mc5.

Chapter 3 investigates the complexes formed by cucurbit[6]uril and primary monoamines using energy resolved SORI CID methods and ion molecule equilibrium measurements. The fragmentation data, branching ratios for the various channels, and the reactivities of the complexes suggest the complexes have the monoammonium threaded through the cavity of CB6 forming a pseudorotaxane architecture. Reactivity studies of complexes of cucurbit[7]uril reveal behaviors distinctive from CB5, mc5 or CB6, which suggests both internally-bound and externally-bound structures are present in CB7 complexes.

Keywords: cucurbituril complexes, SORI, equilibrium, FT ICR MS

ACKNOWLEDGEMENTS

I would like first of all to express sincere appreciation to my instructor, Dr. David V. Dearden. Without his guidance, support, encouragement, and patience, it would be impossible for me to accomplish this work.

I would like to give special thanks to my committee members, Dr. Daniel Austin and Dr. John Lamb, for their advice and help through my research and progress reports. The Department of Chemistry and Biochemistry at Brigham Young University provides the financial support for my graduate studies, and I really appreciate their support.

I gratefully thank my group members, Nannan Fang and Fan Yang especially, for their patient guidance and sincere friendship in these years, and Jacob Embley, who performed the majority of the computational work presented in this thesis.

I would like to thank my family, for their great support and encouragement.

TABLE OF CONTENTS

LIST OF FIGURES

LIST OF TABLES

Chapter 1

Characterization of Supramolecular Assemblies in the Gas Phase using Fourier Transform Ion Cyclotron Resonance Mass Spectrometry

Introduction

Molecular devices built from single molecules or supramolecular assemblies are becoming one of the most promising research areas.[1] Weak, noncovalent interactions and "mechanical" or interlocking bonds are generally responsible for controlling assembly of supramolecular complexes. Thus, understanding the assembly mechanisms of these interactions, the conformations of the supramolecular assemblies, and mechanical fit of the molecular components, is of great importance. There is a great need to develop techniques for characterizing these supramolecular systems.

Techniques typically used to characterize supramolecular assemblies include imaging, NMR, UV-vis and IR spectroscopy, thermogravimetry, X-ray crystallography, and electrospray mass spectrometry.[2] However, many of the systems of interest in supramolecular chemistry are difficult to characterize by the methods listed above. For instance, many interesting complexes do not form crystals, preventing the use of X-ray techniques, and are not suitable for NMR studies because of solubility issues or the presence of magnetic nuclei or insufficient sample.[3] Besides, all of these methods are strongly influenced by the presence of solvent or other matrix materials.

Many examples illustrate that supramolecular behaviors can be masked by the influence of neighboring molecules. The gas phase provides unique insights on the chemistry of

supramolecular complexes. Both solvent and counterion effects can be completely eliminated in the gas phase and the intrinsic interactions in the system are directly shown in the experimental results. Without gas phase work, it is difficult to pin down how condensed phase factors affect the system. In addition, gas phase work allows for direct comparison of experimental results with predictions from high level theory. Finally, the gas phase behavior of these systems is of great interest in its own right, and may have spin-off applications in such diverse areas as modifying the behavior of peptide fragmentation to assist in proteomics studies.

Mass spectrometry remains one of the key tools for performing studies on gas phase species, and is increasingly being applied to supramolecular systems.[4] However, mass spectrometry is primarily used only for detection of the molecular ion corresponding to a supramolecular structure; it is seldom used for full characterization of supramolecular systems. Although measuring the mass of the supramolecular ion yields useful information, that information alone is often not enough to determine the conformational structure of the supramolecular ion, thus it is not able to distinguish between a potentially valuable piece of molecular machinery and a non-specific adduct that is a mass spectrometric artifact arising from the process of transferring the system into vacuum. The work described below aims at exploiting mass spectrometry-based techniques for characterizing the structure and behavior of supramolecular systems in the gas phase, with particular emphasis on cucurbituril complexes. High-level computational modeling of the same systems complements the experimental work. These techniques can also be directly applied to biomolecular studies.

Cucurbituril family

The chemistry of cucurbiturils is gaining increasing interest because of their potential applications in supramolecular structures,[5-6] drug encapsulation, protection, and delivery.[7] The first cucurbituril molecule was synthesized by Behrend *et al*. in 1905 from condensation of urea with glyoxal and formaldehyde.[8] But the pumpkin-shaped molecular structure of cucurbituril was not found until 1981 by Mock *et al*.[9] Now cucurbiturils comprise a family of compounds, commonly written as cucurbit[n]uril, hereafter abbreviated as CBn, where n is the number of repeat units.

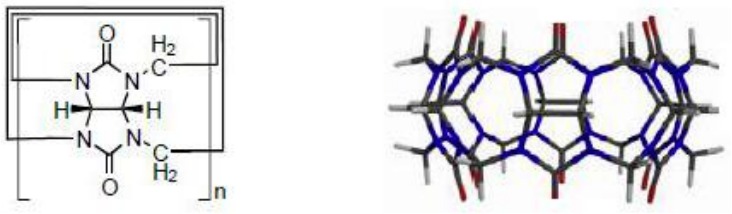

Figure 1.1.[9] Chemical structure of cucurbit[n]uril.

Cucurbituril is a pumpkin-shaped, hollow molecule as shown in Figure 1.1, serving as a sub-nanoscale cage. Crystal structures of cucurbituril homologues characterized by Kim's group are shown in Figure 1.2.[10] Table 1.1[10] shows the dimensional parameters of CB5, CB6 and CB7. The sizes of hollow cavities and portals increase as the number of repeating units increases.

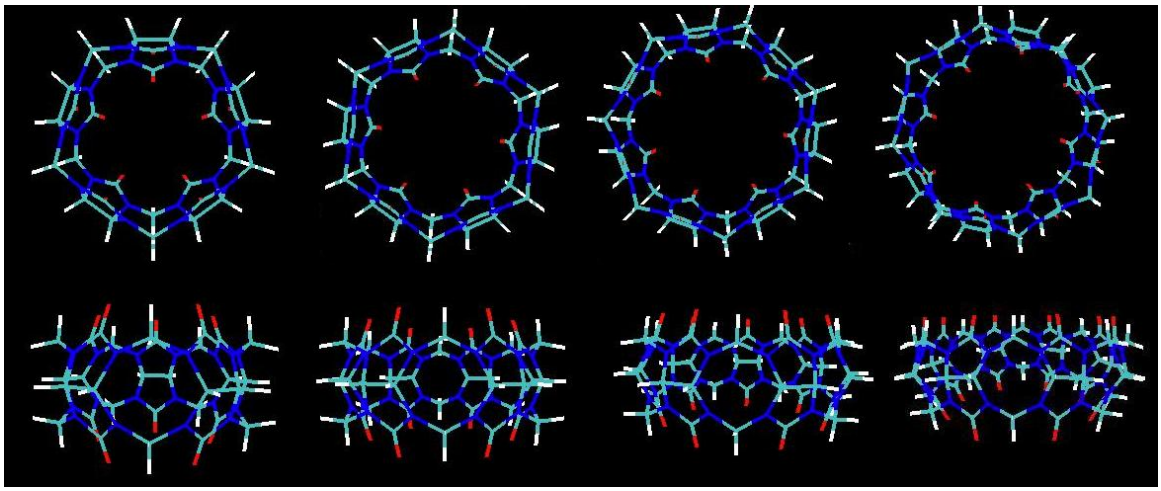

Figure 1.2.[10] X-ray crystal structures of CBn (n = 5-8).

	CB5	CB6	CB7
Outer diameter a (Å)	13.1	14.4	16.0
Inner cavity size b (Å)	4.4	5.8	7.3
Portal size c (Å)	2.4	3.9	5.4
Height d (Å)	9.1	9.1	9.1
Cavity Volume ($Å^3$)	82	164	279

Table 1.1.[10] Dimensional parameters of CBn (n = 5-7).

The greatest limitation to the wide application of cucurbiturils is poor solubility in water. CB6 and CB8 are essentially not soluble, while CB5 and CB7 have modest solubility ($2\text{-}3\times10^{-2}$ M) in water.[11] Recent synthetic advances have led to functionalized cucurbiturils,[12] making the cucurbiturils considerably more soluble in water and organic solvents and thus more suitable for applications.

One of the hallmark features of cucurbituril is its ability of selectively binding ionic species or neutral molecules through noncovalent interactions at the two portals and inside the cavity,[13-15] forming external complexation and inclusion complexation, respectively. The inclusion complexes are denoted following the notation of Smalley,[16] with the "@" symbol indicating inclusion of the species. How can inclusion complexes be distinguished from external complexes? Two mass spectrometry-based techniques are presented below to characterize the structure and behavior of cucurbituril complexes.

Fourier transform ion cyclotron resonance mass spectrometry

Fourier transform ion cyclotron resonance mass spectrometry (FTICR MS) is the tool we use for probing the structures and behaviors of cucurbituril complexes in the gas phase. Among mass spectrometric methods, FTICR MS has the unique ability of trapping ions for extended periods. Thus, ions can be trapped electromagnetically for periods of up to hours, allowing them to undergo many collisions with neutrals even at low pressure and making the attainment of equilibrium possible. Besides, other features of FTICR, such as adaptability to various external ionization sources, high mass measurement accuracy, ultra-high mass resolving power, and versatile tandem mass spectrometry techniques available for straightforward identification of molecules, also make it an attractive technique for the study of large host-guest systems.

FTICR mass spectrometer.

FTICR mass spectrometry became an attractive technique when Marshall *et al.* applied FT methods to previous ICR work in 1974.[17] More than 775 FTICR MS instruments, with a replacement value of approximately $450 million, have been installed in laboratories worldwide since its invention. The schematic of a general FTICR mass spectrometer is shown in Figure 1.3.[18]

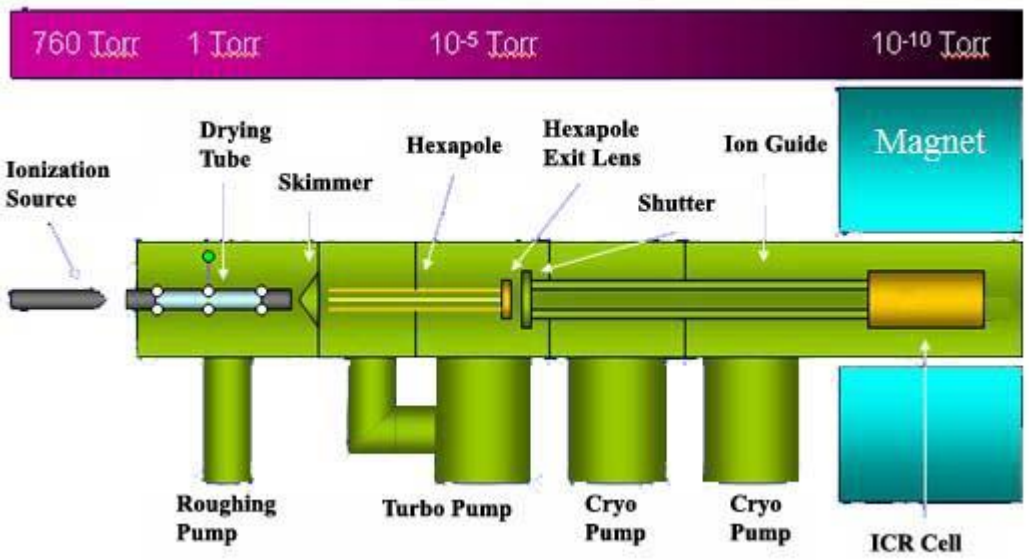

Figure 1.3.[18] The schematic of a general FTICR mass spectrometer.

The instrument is typically composed of the following parts: ionization source, ion guide optics, mass analyzer and data analysis device. Gas phase ions are generated by an ionization source, transferred through ion guide optics by applying a series of voltage differences, and then injected into the ICR trapping cell, where ion excitation and detection happen.

In the early days, internal ionization dominated the FTICR MS instrument due to its simplicity. With the increasing need for examining nonvolatile samples and the development of ion guide and ion cooling techniques, coupling external ionization sources with FTICR MS became more popular. Two common external ionization sources used in FTICR MS instruments are electrospray ionization (ESI)[19-20] and matrix-assisted laser desorption/ionization (MALDI).[21]

Ion guide optics perform the transferring of ions from high pressure (usually 1 atm) to a pressure of 10^{-9} mbar or lower. Usually three or four differential pumping stages are required to guarantee this pressure drop. High capacity pumps such as cryogenic pumps and turbo pumps are utilized to achieve ultra-high vacuum. High vacuum is preferable because collisions between the desired ions and air molecules can result in a loss of coherent motion.

The ICR trapping cell, the heart of the FTICR MS instrument, is the place that ion storage, ion selection, ion reaction or dissociation and ion analysis take place. It is located inside a uniform static superconducting high field magnet cooled by liquid helium and liquid nitrogen. Ultra-low pressure in the ICR trapping cell, $10^{-8} – 10^{-9}$ Torr, is required during ion excitation and detection to achieve high resolving power and mass accuracy.

The strength of the magnetic field can influence the performance of FTICR MS in many aspects, such as mass resolving power, data acquisition speed and upper mass limit.[22] Magnetic

field strength has developed from 1.4 T in the mid 1960s to 21 T (superconducting system is in the development phase) in 2011.[23]

Ion motion in the ICR trapping cell.

When ions are injected into the trapping cell, three different types of ion motion occur: cyclotron motion, trapping oscillation, and magnetron motion. The ion cyclotron motion is shown in Figure 1.4.[22] The cyclotron motion in the x-y plane is confined by the spatially homogenous and axially directed magnetic field in the z direction. Cyclotron frequency is only dependent on the magnetic field and mass to charge ratio. Thus, ions of the same *m/z* will have the same cyclotron frequency.

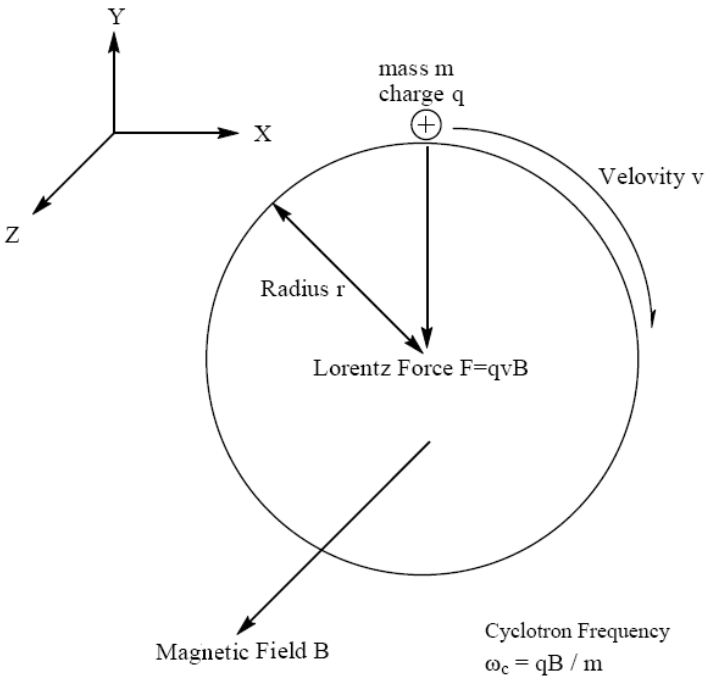

Figure 1.4.[24] Ion cyclotron motion

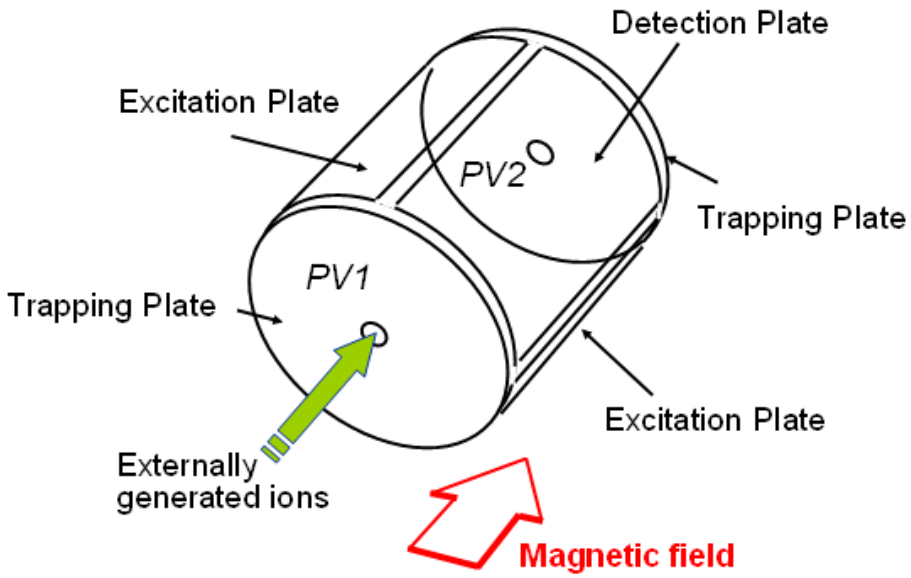

Figure 1.5.[18] Schematic of a cylindrical ICR trapping cell.

Figure 1.5 is a schematic of a cylindrical ICR trapping cell. It is composed of trapping plates, excitation plates and detection plates. Ions are injected along the magnetic field direction and can fly out of the cell quickly if there is no force along the z direction applied to them. In order to trap them in the cell, an electric potential is applied onto the trapping plates. However, the electric potential will cause the ions to move in a harmonic oscillation between the two trapping plates, and the combination of radial electric field and magnetic field will result in the magnetron motion of the ions, shown in Figure 1.6. Therefore, the theoretical cyclotron frequency needs to be modified, which is shown in Eqn. (1). ω_t is the frequency of the electric potential, and ω_c' is the modified cyclotron frequency.

$$\omega_c' = \omega_c / 2 + [(\omega_c / 2)^2 - (\omega_t / 2)^2]^{1/2} \quad (1)$$

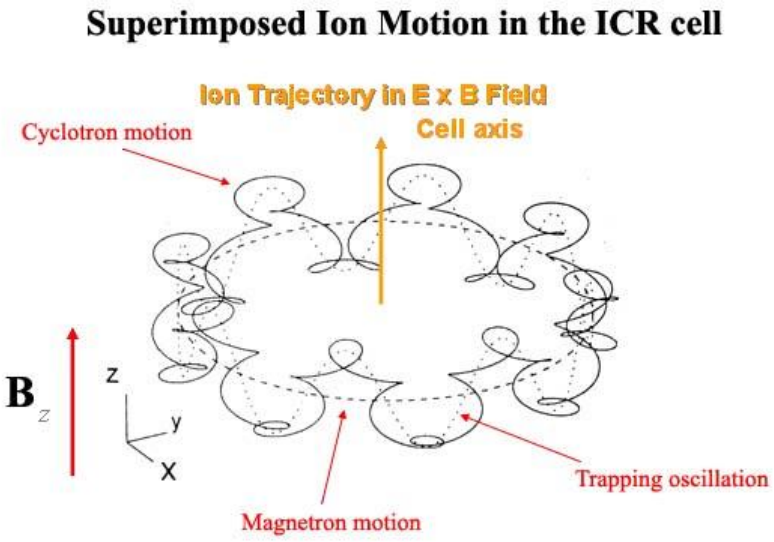

Figure 1.6.[18] Schematic of superimposed ion motion in the ICR cell.

The ion cyclotron frequency can be determined by measuring the image current produced on the detection plates of the trapping cell by the orbiting ions. However, ions injected in the ICR trapping cell have very small initial orbit radii and cannot produce a detectable image current. A radio frequency (RF) pulse is applied to the transmitter plates of the trapping cell. Ions that absorb RF energy will be accelerated into larger orbits and ions of the same *m/z* will be excited into a coherent packet and produce detectable image current, which is a time domain waveform. By performing a Fourier transform, the time domain signal is changed into a frequency domain spectrum.

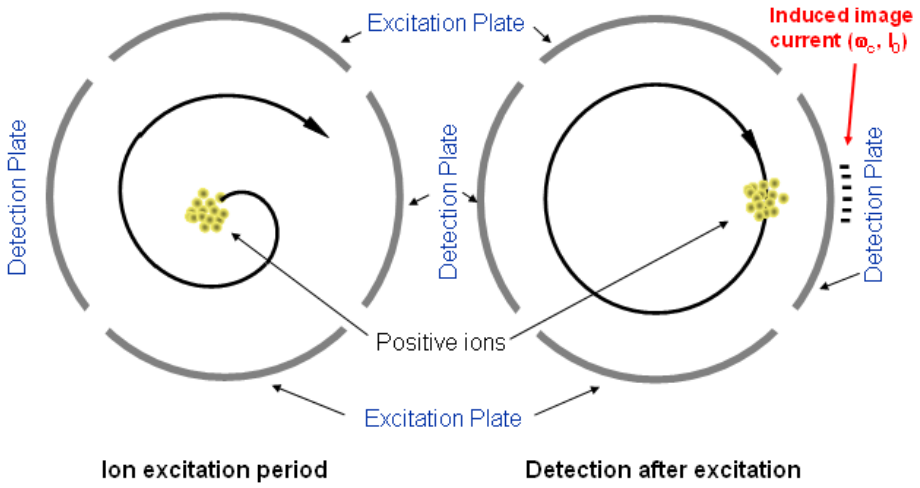

Figure 1.7.[18] Ion excitation and detection in the ICR cell.

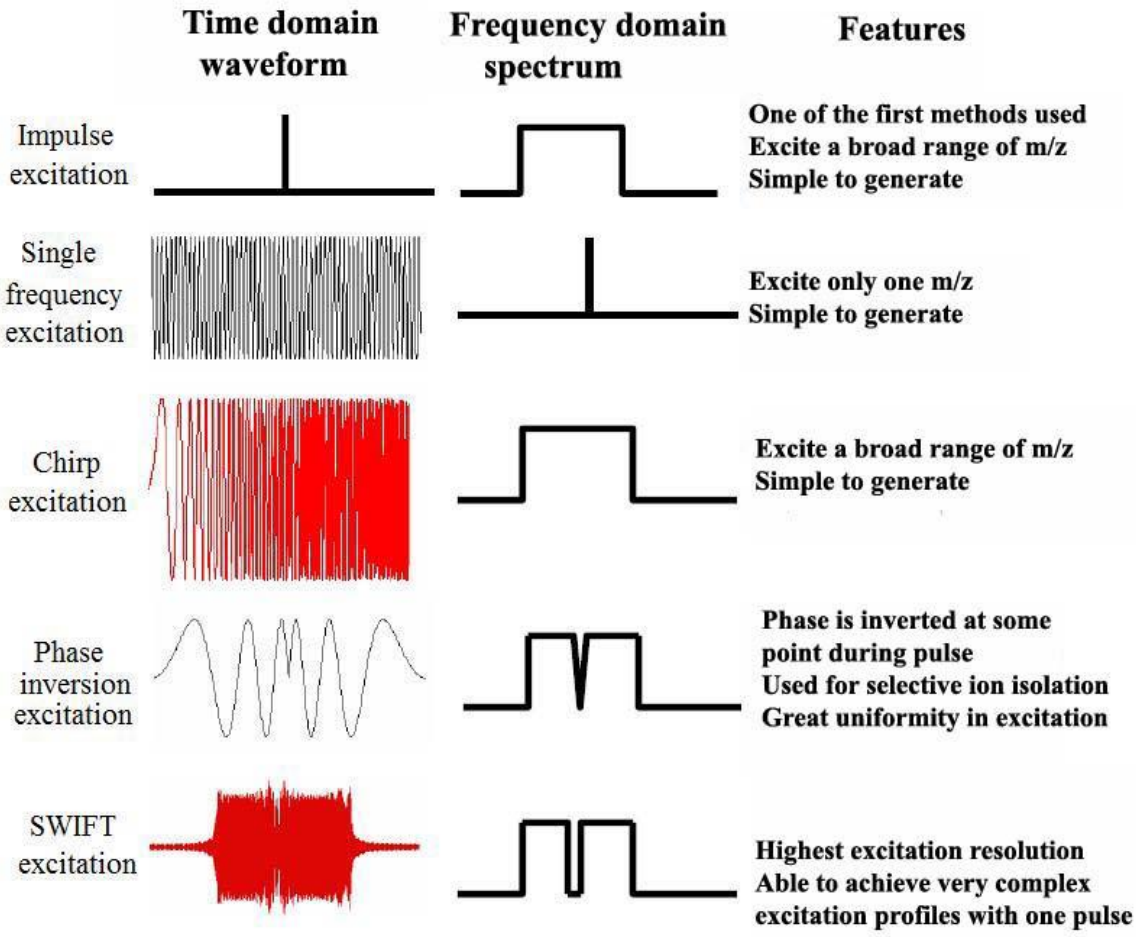

Figure 1.8.[24] Excitation pulses used in FTICR mass spectrometry.

Several types of excitation pulse used in FTICR mass spectrometry are shown in Figure 1.8. Impulse excitation[25] is an early method used for broad range excitation. Chirp excitation[17] is one of the most widely used excitation methods. Stored waveform inverse Fourier transform (SWIFT) excitation[26-28] was invented by Marshall's group in 1985. It is believed SWIFT has the greatest power uniformity as a function of frequency and yields the greatest frequency resolution. The ion excitation function can also be used for increasing ion kinetic energy above the collision-activated dissociation threshold and ejecting the ions from the trap.

Mass spectrometry-based methods for supramolecular characterization

Versatile tandem mass spectrometry capabilities (MS^n) greatly contribute to the structural analysis ability of FTICR MS in dealing with supramolecular system. During tandem mass spectrometry, ions are activated, and then allowed to react or dissociate in different ways to produce secondary ions. The secondary ions are detected and analyzed to give information about the parent ion. Table 1.2 shows a few dissociation techniques used in tandem mass spectrometry.

SORI CID[29]	Sustained Off-Resonance Irradiation Collision Induced Dissociation
SID[30]	Surface Induced Dissociation
UVPD[31]	Ultraviolet Photodissociation
IRMPD[32]	Infrared Multiphoton Photodissociation
BIRD[33]	Blackbody Infrared Radiative Dissociation
ECD[34]	Electron Capture Dissociation

Table 1.2. Dissociation techniques for tandem FT ICR mass spectrometry.

Sustained off-resonance irradiation collision induced dissociation.

Characterization of dissociation products is a typical way of probing supramolecular ions in mass spectrometry. Sustained off-resonance irradiation collision induced dissociation[29] (SORI CID) is routinely used to cause dissociation of supramolecular systems due to its mild, multiple-collision nature. During the SORI process, molecular ions are mildly activated by an off-resonant RF excitation and are allowed to collide with background gas to produce secondary ions. Energy gradually adds to the molecular ions through many low energy collisions with background gas rather than through a single high-energy collision. Therefore, the lowest energy dissociation channels are selectively populated.

If the energy supplied to ions during the SORI process can be quantified relatively, meaningful comparison of the relative dissociation thresholds of these molecular ions will be established, yielding structural and energetic information for the supramolecular system.

The amount of energy deposited in the ion via the SORI event, written as E_{SORI}[35], depends on the average energy transferred per collision, E_{coll}, and the number of collisions the ion undergoes, n_{coll}, as shown in Eqn. (2).

$$E_{\mathrm{SORI}} = n_{\mathrm{coll}} E_{\mathrm{coll}} \tag{2}$$

Laskin and Futrell have successfully used SORI to quantitatively characterize the dissociation of bromobenzene[36] and bromonaphthalene[37] ions, and derived an expression for the maximum kinetic energy in the center-of-mass reference frame during SORI, shown in Eqn. (3).[37]

$$E_{\mathrm{CM}}^{\max} = \frac{\beta^2 q^2}{32\pi^2 d^2 (\Delta f)^2} \left(\frac{M}{M+m}\right) \frac{V_{\mathrm{pp}}^2}{m} \tag{3}$$

In this expression, β is the geometry factor of the trapping cell, q is the charge on the ion, d is the trapping cell diameter, Δf is the frequency offset of the excitation pulse from the ion's

resonant frequency, M is the mass of the neutral, m is the mass of the ion, and V_{pp} is the peak-to-peak amplitude of the SORI excitation pulse.

We assume the average energy transferred per collision in the center-of-mass frame of reference, E_{coll}, is a constant fraction of the maximum kinetic energy and the fraction is f_E,[38] shown in Eqn. (4).

$$E_{coll} = f_E E_{CM}^{max} \tag{4}$$

The number of collisions the ion undergoes, n_{coll}, is a function of the collision time, t_{coll}, expressed in Eqn. (5).[38] N^* is the product of neutral gas number density, σ is collision cross section and K_v is the proportionality constant relating the average ion velocity to maximum ion velocity.

$$n_{coll} = N^* \sigma K_v \frac{\beta q}{4\pi d \Delta f} \frac{V_{pp}}{m} t_{coll} \tag{5}$$

An expression for E_{SORI} can be obtained by combining Eqns. (2), (3), (4) and (5), shown as follows. All the terms except σ, M, m, V_{pp} and t_{coll} are constant.

$$E_{SORI} = N^* \sigma K_v f_E t_{coll} \frac{\beta^3 q^3}{128\pi^3 d^3 (\Delta f)^3} \left(\frac{M}{M+m}\right) \frac{V_{pp}^3}{m^2} \tag{6}$$

E_{SORI} can be varied by varying the amplitude of the SORI excitation, by varying the duration of the SORI event, or by varying the pressure and/or mass of the background gas. Heeren's work[35] makes a strong case that the best way to vary SORI energy is by varying the length of the SORI event. In this way, V_{pp} in Eqn. (6) becomes constant and the expression can be simplified into Eqn. (7). E_{SORI} is proportional to the time during which collisions take place, t_{coll}, which is also the length of the SORI event.

$$E_{SORI} \propto \left(\frac{M}{M+m}\right) \frac{\sigma}{m^2} t_{coll} \tag{7}$$

The relative E_{SORI} can be determined using Eqn. (7). Relative collision cross sections are estimated by computing the solvent accessible surface areas. By varying the duration of the SORI event and maintaining other parameters such as SORI excitation amplitude the same, we can obtain dissociation threshold information from a set of mass spectra with different dissociation ratios of the supramolecular ions. The relative dissociation thresholds, compared with computational results, yield structural information about the supramolecular system.

Reactivity of supramolecular ions.

The structure and behavior of a supramolecular system can also be characterized through its reactivity with other species. The reactivity of supramolecular ions can be studied through exchange reactions with gaseous neutrals at low pressures. Such an exchange reaction is generically described as

$$XY^+ + Z \underset{k_r}{\overset{k_f}{\rightleftharpoons}} ZY^+ + X$$

The exchanged species Y^+ is a supramolecular ion, and X and Z are neutrals. At low pressures and typical thermal energies, the stoichiometric coefficients for ionic species XY^+ and ZY^+ are always unity because Coulombic repulsion prevents reactive collisions between ions. The stoichiometric coefficients for neutrals X and Z are generally unity because the probability of three body collisions is small at low pressure. It is frequently possible for ligand-exchange on a cucurbituril host to reach equilibrium. Therefore, the reaction above is written for the equilibrium state.

For the reactions of neutral ideal gases A and B to give ideal gas products C and D, it is straightforward to show the equilibrium constant expression, K_P, in Eqn. (8). This derives from

the fact that the chemical potential of reactants is equal to that of products at equilibrium. P_R is the partial pressure (in bars) of species R at equilibrium, and P is the standard-state pressure defined for neutral gases (1 bar).

$$aA + bB \rightleftarrows cC + dD$$

$$K_P = \frac{(\frac{P_C}{P})^c (\frac{P_D}{P})^d}{(\frac{P_A}{P})^a (\frac{P_B}{P})^b} \tag{8}$$

The extension of Eqn. (8) to ion-molecule reactions requires the definition of a standard state for ions analogous to the standard-state pressure defined for neutral gases. The standard state defined for an ionic species is defined as the hypothetical state where the ion number density is the same as the number density of neutral gas particles at 1 bar pressure. Therefore, the equilibrium constant, K, for ion-molecule reaction at low pressure is given by

$$K = \frac{\frac{n_{ZY^+}}{n}\frac{P_X}{P}}{\frac{n_{XY^+}}{n}\frac{P_Z}{P}} \tag{9}$$

n_R is the number density of ionic species R^+ at equilibrium and n is the number density of ions equal to that of neutral particles at 1 bar pressure. Since the units used to express ion number densities and neutral pressures are cancelled, the equilibrium constant, K, is a dimensionless quantity.

One approach to determining the equilibrium constant is measuring the parameters in Eqn. (9). This method involves measurements of the relative abundances of ionic reactant and product under equilibrium conditions, as well as determination of the pressures of the neutral reactant

and product. The relative abundance ratio of ionic species is typically taken from ratio of peak heights or areas in the mass spectrum. Although mass discrimination between reactant and product may cause error in the measurement of equilibrium constants, errors in thermochemistry are generally small because of the logarithmic relationship between K and the standard Gibbs free energy change. Measurement of the neutral pressures involves correction for their different gauge sensitivities.[39] It is crucial to verify the system actually reaches equilibrium when using this approach. Two criteria are generally applied. First, the ratio of reactant to product abundances must be constant with time within experimental error. However, this constant ratio is not sufficient to prove the system is at equilibrium, especially when reaction rates are slow as reactions often occur at low pressures. A better check for equilibrium involves re-establishment of the same abundance ratio when a system presumed to be at equilibrium is perturbed by partial ejection of either the ionic reactant or the ionic product regardless of the direction of the perturbation.

Another approach is to measure the forward k_f and reverse k_r rate constants for the reaction, as the equilibrium constant can also be expressed in Eqn. (10).

$$K = \frac{k_f}{k_r} \tag{10}$$

If the pressures of the neutrals, X and Z, are constant during the reaction and the number densities of the neutrals are much higher than those of the ionic species, XY^+ and ZY^+, the forward and reverse reactions become pseudo-first order reactions and only depend on the number densities of the ionic species as illustrated in Eqn. (11).

$$r_f = k_f[\mathrm{XY}^+][\mathrm{Z}] = k_f'[\mathrm{XY}^+]$$
$$r_r = k_r[\mathrm{ZY}^+][\mathrm{X}] = k_r'[\mathrm{ZY}^+] \quad (11)$$

The abundances of reactant and product ions are measured independently as a function of time. Thus, k_f' and k_r' are determined. k_f and k_r can be obtained by dividing k_f' and k_r' with the corresponding number densities of neutrals. This approach has the advantage that it is not necessary to actually achieve equilibrium, so long as it can confidently be established that the identity and rates of the forward and reverse reactions are correct.

Equilibrium and thermochemistry are intimately connected. The equilibrium constant, K, is directly related to standard Gibbs free energy change ΔG° through Eqn. (12), where R and T are the ideal gas constant and absolute temperature.

$$\Delta G^\circ = -RT \ln K \quad (12)$$

Exchange reactions involve breaking bonds to one species and formation of bonds with another. Therefore, measurement of exchange equilibrium does not directly yield absolute binding thermochemistry data, but rather gives the free energy change in the reaction.

Equilibrium is an excellent method for probing two systems that have small energy differences. Take exothermic reactions for instance. When bonds are formed at low pressure, the energy released resides in the product and is sufficient to break the nascent bond unless it is disposed of in some way, such as collisional or radiative channels. The magnitude of the free energy change in a reaction generally must be less than about 15-20 kJ/mol for equilibrium to be observable with FTICR instrumentation.

References

(1) Newton, D.E. *Recent Advances and Issues in Molecular Nanotechnology*; Greenwood Press: Westport (CT), 2002.

(2) Smith, R. D.; Loo, J. A.; Loo, R. R. O.; Busman, M.; Udseth, H. R. *Mass Spectrom. Rev.***1991**, *10*, 359-451.

(3) Steed, J. W.; Atwood, J. L. *Supramolecular Chemistry;* 2nd ed.; Wiley: Chichester (UK), 2009.

(4) Schalley, C. A. *Int. J. Mass Spectrom*. **2000**, *194*,11-39.

(5) Nau, W. M.; Hennig, A.; Koner, A. L. *Springer Ser. Fluoresc.***2008**, *4*, 185-211.

(6) Hwang, I.; Ziganshina, A. Y.; Ko, Y. H.; Yun, G.; Kim, K. *Chem. Commun.* **2009**, 416-418.

(7) Wheate, N. J. *J. Inorg. Biochem.* **2008**, *102*, 2060-2066.

(8) Behrend, R.; Meyer, E.; Rusche, F.; *Liebigs Ann. Chem*. **1905**,*339*,1.

(9) Freeman, W. A.; Mock, W. L.; Shih, N.-Y. *J. Am. Chem. Soc.* **1981**, *103*, 7367.

(10) Kim, J.; Jung, I.-S.; Kim, S.-Y.; Lee, E.; Kang, J.-K.; Sakamoto, S.; Yamaguchi, K.; Kim, K. *J. Am. Chem. Soc.* **2000**, *122*, 540-541.

(11) Lee, J. W.; Samal, S.; Selvapalam, N.; Kim, H.-J.; Kim, K. *Acc. Chem. Res.* **2003,** *36*, 621-630.

(12) Kim, K.; Selvapalam, N.; Ko, Y. H.; Park, K. M.; Kim, D.; Kim, J. *Chem. Soc. Rev.* **2007**, *36*, 267-279.

(13) Buschmann, H. J.; Jansen, K.; Schollmeyer, E. *Acta Chim. Slov*. **1999**, *46*, 405-411

(14) Lagona, J.; Mukhopadhyay, P.; Chakrabarti, S.; Isaacs, L. *Angewandte Chemie International Edition* **2005**, *44*, 4844-4870

(15) Ong, W.; Kaifer, A. E. *J. Org. Chem*. **2004**, *69*, 1383-1385

(16) Chai, Y.; Guo, T.; Jin, C. M.; Haufler, R. E.; Chibante, L. P. F.; Fure, J.; Wang, L. H.; Alford, J. M.; Smalley, R. E. *J. Phys. Chem.* **1991**, *95*, 7564-7568.

(17) Comisarow, M. B.; Marshall, A. G. *Chem. Phys. Lett.* **1974**, *25*, 282.

(18) Guo, Y. http://www.lab.org.cn/UserFiles/FTICRMS(1).doc.

(19) Yamashita, M.; Fenn, J. B. *J. Phys. Chem.* **1984**, *88*, 4451-4459.

(20) Yamashita, M.; Fenn, J. B. *J. Chem. Phys.* **1984**, *88*, 4671-4675.

(21) Karas, M.; Bachmann, D.; Bahr, U.; Hillenkamp, F. *Int. J. Mass Spectrom. and Ion Proc.* **1987**, *78*, 53.

(22) Marshall, A. G.; Hendrickson, C. L.; Jackson, G. S. *Mass Spectrom. Rev.* **1998**, *17*, 1-35.

(23) http://www.magnet.fsu.edu/mediacenter/features/meetthemagnets/fticr.html.

(24) Dearden, D. V. FT-ICR-MS Tutorial Presentation.

(25) Mclver R. T., B. G., Hunter R. L. *Int. J. Mass Spectrom* **1989**, *89*, 489-491.

(26) Marshall, A. G.; Wang, T. C.; Ricca, T. L. *J. Am. Chem. Soc.* **1985**, *107*, 7893-7897.

(27) Goodman, S., Hanna, R.: U.S. Patent, **1986**, No. 4945234.

(28) Guan, S.; Marshall, A. G. *Anal. Chem.* **1993**, *65*, 1288-1294.

(29) Gauthier, J. W.; Trautman, T. R.; Jacobson, D. B. *Anal. Chim. Acta* **1991**, *246*, 211-225.

(30) Castoro, J. A.; Nuwaysir, L. M.; Ijames, C. F.; Wilkins, C. L. *Anal. Chem.* **1992**, *64*, 2238-2243.

(31) Bowers, W. D.; Delbert, S. S.; Hunter, R. L.; Mclver, R. T. *J. Am. Chem. Soc.* **1984**, *106*, 7288.

(32) Little, D. P.; Chorush, R. A.; Speir, J. P.; Senko, M. W.; Kelleher, N. L.; McLafferty, F. W. *J. Am. Chem. Soc.* **1994**, *116*, 4893-4897.

(33) Dunbar, R. C.; McMahon, T. B. *Science* **1998**, *279*, 194-197.

(34)Xu, L. X.; Huang, Y. L.; Giese, R. W. *Journal of Mass Spectrometry* **1998**, *33*, 615-620.

(35) Guo, X.; Duursma, M. C.; Al-Khalili, A.; Heeren, R. M. A. *Int. J. Mass Spectrom*. **2003**, *225*, 71.

(36) Laskin, J.; Byrd, M.; Futrell, J. *Int. J. Mass Spectrom.* **2000**, *195/196*, 285.

(37) Laskin, J.; Futrell, J. *J. Phys. Chem.* **2000**, *104*, 5484.

(38) Zhang, H.; Ferrell, T. A.; Asplund, M. C.; Dearden, D. V. *Int. J. Mass Spectrom*. **2007**, *265*, 187-196.

(39) Bartmess J. E.; Georgiadis R. M., *Vacuum* **1983**, *33*, 149-153.

Chapter 2

Characterization of alkylmonoammonium complexes with cucurbit[5]uril and decamethylcucurbit[5]uril in the gas phase

Introduction

Cucurbiturils, named after the Latin for the pumpkin family, are pumpkin-shaped, hollow molecules. Cucurbiturils comprise a family of compounds, commonly written as cucurbit[n]uril, hereafter abbreviated as CBn, where n is the number of repeat units. As shown in Figure 2.1, cucurbiturils have two carbonyl-lined portals that form ideal binding sites for positive ions, and an interior cavity that can accommodate molecules of the proper size and shape. Recent synthetic advances have led to functionalized cucurbiturils[1-3], making the cucurbiturils considerably more soluble in water and organic solvents and thus more suitable for applications.

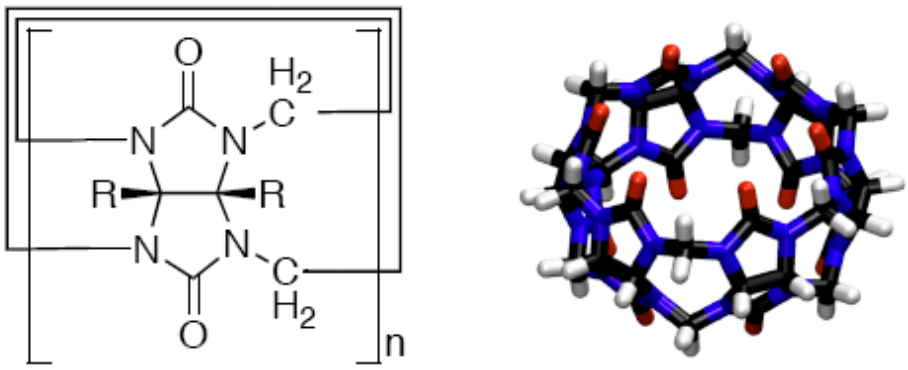

Figure 2.1. Left: chemical structure for cucurbit[n]uril. R = H for CBn; R = CH_3, n = 5 for mc5. Right: a model of cucurbit[6]uril (gray = carbon, red = oxygen, blue = nitrogen, white = hydrogen).

Decamethylcucurbit[5]uril, hereafter referred to as mc5, is the methyl-substituted analog of cucurbit[5]uril. It has been found that CB5 and mc5 can be used in combination with ammonium ions[4] or alkali metal cations[5] to form supramolecular containers, trapping small molecule as "prisoners" in their hollow interior cavities, with the cucurbituril serving as the walls of the container and the ammonium ions or metal cations serving as "lids". An example of this supramolecular nanobox is shown in Figure 2.2.

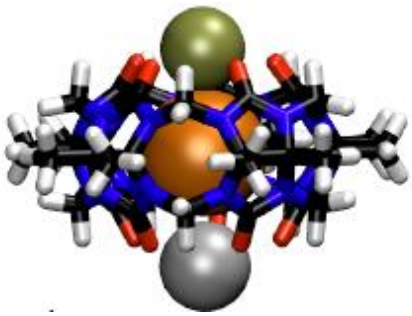

Figure 2.2. Decamethylcucurbit[5]uril (mc5), bound to Na^+ (top) and K^+ (bottom) to form a molecule nanobox trapping a Xe atom (orange) inside.

Primary alkylammonium ions also likely make good lids for CB5 and mc5 nanoboxes. The alkylammonium ions tend to insert their alkyl tails into the cucurbituril cavity in solution, due to the entropic benefit of releasing solvent from the cavity.[6] Jansen et al.[7] have found that CB5 forms internal complexes with primary alkylammonium ions in solution while the relatively rigid mc5 only forms external complexes. What type of complex between CB5 or mc5 and alkylmonoammonium ions will prevail in the gas phase, where the entropic driving force of releasing solvent is not present?

Previous studies on the complex formed by CB6 with 1,4-butanediamine show that external and internal complexes exhibit distinctive collision-induced dissociation and reactivity properties.[8] Complexes with internal diamine structures react with propylamine via slow addition,

whereas complexes with externally-bound diamine structures react via rapid amine exchange. In addition, collisional activation and dissociation of the internal complexes is relatively difficult (requires higher energies) and the complex tends to dissociate via covalent cleavages, whereas external complexes dissociate with low-energy collisional activation via simple loss of the amine.

Here we investigate the conformational structure of complexes formed by CB5 or mc5 with alkylmonoammonium ions using electrospray ionization Fourier transform ion cyclotron resonance mass spectrometry (ESI-FTICR/MS). Both the collision induced dissociation behavior of these complexes and their reactivity with neutral amines will be studied to characterize these supramolecular complexes. In addition, these studies are complemented by high-level computational modeling of the same systems.

Experimental Section

ESI mass spectrometry. Collision-induced dissociation experiments were carried out using a Fourier transform ion cyclotron resonance mass spectrometer[9] (model APEX 47e; Bruker Daltonics; Billerica, MA) equipped with a 4.7 Tesla superconducting magnet. This instrument was controlled by a MIDAS data system,[10] and experimental data were processed using the Igor Pro data analysis package (version 6.04; WaveMetrics; Lake Oswego, OR).[11] The electrospray ionization source coupled with this mass spectrometer was modified from an Analytica design (model 10413; Analytica, Branford, MA) using a heated metal capillary inlet maintained at about 50 °C. The source was typically operated at a flow rate of 30 μL hr^{-1}, and the spray needle was typically biased at +1.5 kV. Reactivity experiments were carried out on a 9.4 Tesla FT ICR mass spectrometer (model APEX II; Bruker Daltonics; Billerica, MA) equipped with an Apollo™ API

source (Bruker Daltonics; Billerica, MA). An XMASS data system (version 6.0.2; Bruker Daltonics) was used to control this instrument and perform the data analysis. The electrospray source was typically operated at a flow rate of 150 μL hr^{-1}. These values were optimized for intensity and stability of the electrospray signal.

Materials and sample preparation. Alkylmonoamines were purchased from Sigma Chemical Co. (St. Louis MO). Cucurbit[5]uril was obtained from Prof. Kimoon Kim (Pohang University of Science and Technology, Pohang, Republic of Korea).[12] Samples of decamethylcucurbit[5]uril (mc5) were obtained from IBC Advanced Technologies (American Fork, UT).[13] All of the chemicals were used as supplied, without additional purification. Alkylmonoamines were dissolved in pure methanol to a concentration of 5×10^{-4} M. CB5 and mc5 stock solutions were prepared by dissolving solid samples in HPLC grade water (Mallinckrodt Baker Inc., Phillipsburg, NJ) at concentration of 2×10^{-4} M. Electrospray solutions were prepared by mixing 500 μL of the CB5 or mc5 stock solution with 500 μL of the n-alkylmonoamine solution. The final concentration of CB5 or mc5 analyte was 100 μM in the electrospray solutions.

SORI CID Experiments. Collision-induced dissociation (CID) was conducted using the sustained off-resonance irradiation (SORI) method.[14] Stored waveform inverse Fourier transform (SWIFT) techniques[15] were used to isolate ions of interest. Isolation was followed by introducing argon as a collision gas. Ar was introduced using a Freiser-type pulsed leak valve[16] with a backing pressure of 30 psig maintaining during the experiment. In the SORI events, the gas pulsed-valve was activated for 6 ms, yielding an Ar background pressure in the trapping cell of about 1×10^{-5} mbar. Single-frequency 1 kHz off-resonance irradiation was applied to the target ions during the gas pulse. The length of the off-resonance irradiation event was varied

systematically from 1 ms to 500 ms, with the amplitude of the SORI excitation held constant at 38.5 V (measured at the vacuum feedthrough to the trapping cell). Following the SORI event was a 10 s delay to allow the instrument to return to base pressure (10^{-9} mbar) prior to broadband excitation and detection. Three scans were averaged for each SORI duration.

Reactivity experiments. The reactivity of the CB5 and mc5 complex ions with neutral alkylmonoamines was studied by leaking neutral alkylmonoamines into the ion-trapping region of the vacuum chamber through controlled variable leak valves to a constant pressure (~10^{-7} mbar). The partial pressure of each neutral alkylmonoamine was measured using a Granville-Phillips Stabil-Ion gauge. One amine was introduced, the pressure was stabilized and measured, after which the second amine was added, pressure stabilized, and measured. Ionization gauge sensitivities may vary in response to different gases. Therefore, the pressure measured by the Stabil-Ion gauge needs to be corrected.[17] A solution of CB5 or mc5 with one of the alkylmonoamines was electrosprayed. The electrosprayed complex ions were isolated, and then allowed to react with the pair of neutral amines in the trapping cell. The reaction time (between isolation of the ionic reactant and detection of reactants and products) was varied programmatically and the mass spectra were recorded using XMASS. Next the solution of CB5 or mc5 with the other alkylmonoamine was electrosprayed and the whole experimental process was repeated with the same neutral pressures. Three measurements were conducted for each complex.

Computational methods. The structures of the complexes were sketched using the Maestro/MacroModel modeling package (Macromodel version 7.1; Schrödinger, Inc.; Portland, OR). Conformational searches were carried out using the MMFF94S force field[18] with no nonbonded cutoffs and employing the MCMM method with automatic setup. The lowest-energy

structures found in the conformational searches were used as the starting point for B3LYP/6-31+G* geometry optimization. All of these calculations were performed by using the ECCE package[19] (version 3.1; Pacific Northwest National Laboratory; Richland, WA), and used the computational engine of NWChem[20] (version 4.7; Pacific Northwest National Laboratory; Richland, WA).

Results

Electrospray mass spectra.

Solutions of CB5+$CH_3(CH_2)_nNH_2$ and mc5+$CH_3(CH_2)_nNH_2$ (n = 0-7) were each electrosprayed into the 4.7 T FTICR mass spectrometer. For the ESI spectra of CB5+$CH_3(CH_2)_nNH_2$, we observed peaks of singly-charged ions, which are $[CB5+H_3O]^+$ (m/z 849.3) and $[CB5+CH_3(CH_2)_nNH_3]^+$ (m/z range from 862.3 to 960.4), and doubly-charged ions $[CB5+2CH_3(CH_2)_nNH_3]^{2+}$ (m/z range from 447.2 to 545.3). Experimental observation of $[CB5+H_3O]^+$ is significant as H_3O^+ has been proposed as a template ion in the formation of CB5.[21] The electrospray mass spectra of mc5+$CH_3(CH_2)_nNH_2$ are quite similar to those of CB5+$CH_3(CH_2)_nNH_2$, including peaks of singly-charged ions, which are $[mc5+H_3O]^+$ (*m/z* 989.4) and $[mc5+CH_3(CH_2)_nNH_3]^+$ (*m/z* range from 1002.5 to 1100.6), and doubly-charged ions $[mc5+2CH_3(CH_2)_nNH_3]^{2+}$ (*m/z* range from 517.3 to 615.4). All of the singly-charged ions gave sufficient signal to do the SORI-CID experiments.

SORI CID behavior of $[CH_3(CH_2)_nNH_3•CB5]^+$ and $[CH_3(CH_2)_nNH_3•mc5]^+$ (n = 0-7).

Singly-charged ions of $[CH_3(CH_2)_nNH_3•CB5]^+$ and $[CH_3(CH_2)_nNH_3•mc5]^+$ (n = 0-7) were isolated using SWIFT and excited 1 kHz below their resonant frequency. Here pentylamine (n = 4) is chosen as an example. Figure 2.3 shows the SORI CID spectra for $[CH_3(CH_2)_4NH_3•CB5]^+$ (*m/z* 918.4) and $[CH_3(CH_2)_4NH_3•mc5]^+$ (*m/z* 1058.5) complexes. Peaks next to the labeled peak are the isotopic peaks.

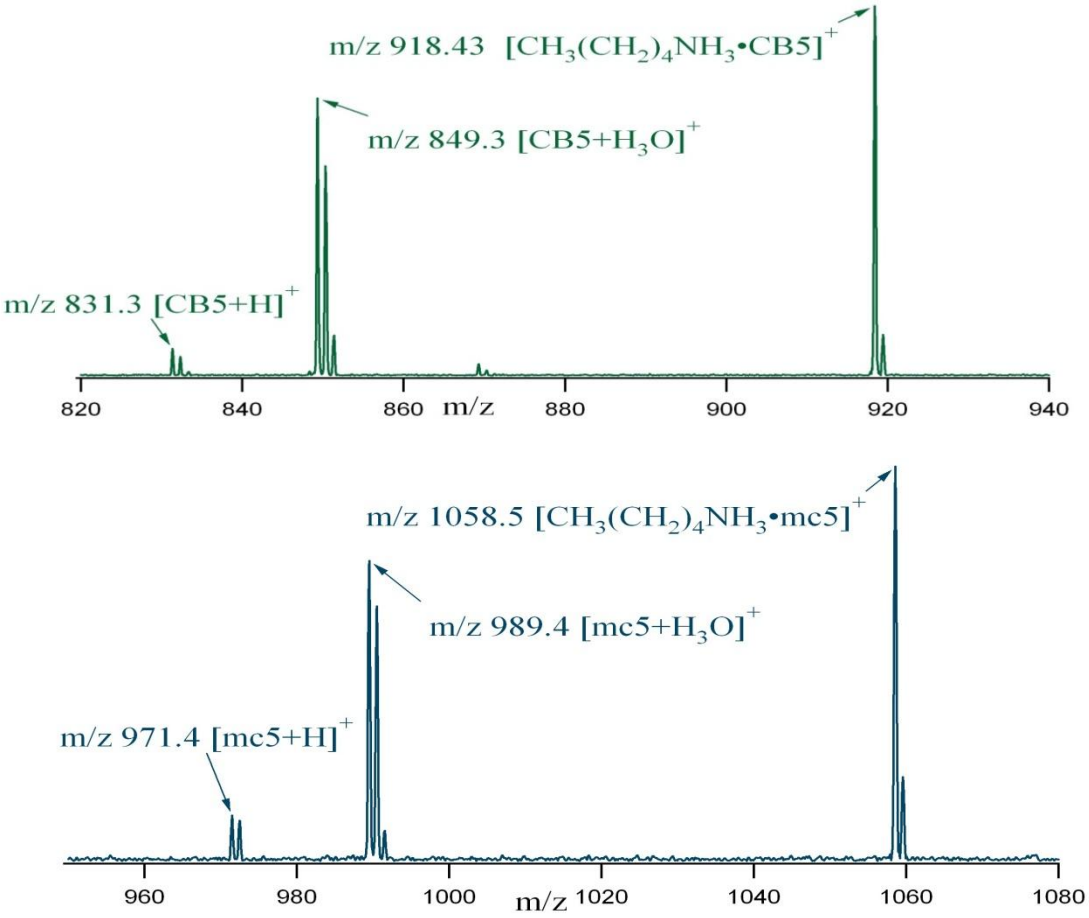

Figure 2.3. Sustained off-resonance irradiation collision-induced dissociation spectra of $[CH_3(CH_2)_4NH_3•CB5]^+$ (125 ms irradiation) and $[CH_3(CH_2)_4NH_3•mc5]^+$ (175 ms irradiation). These were both excited on the high mass side, so the higher mass isotopes of the reactants are depleted and those of the products are enhanced.

In both the $[CH_3(CH_2)_4NH_3•CB5]^+$ and $[CH_3(CH_2)_4NH_3•mc5]^+$ SORI CID spectra, only two dissociation products are evident. The dissociation products of $[CH_3(CH_2)_4NH_3•CB5]^+$ are located at *m/z* 831.3 and *m/z* 849.3, corresponding to $[CB5+H]^+$ and $[CB5+H_3O]^+$. The two dissociation products of $[CH_3(CH_2)_4NH_3•mc5]^+$ are $[mc5+H]^+$ at *m/z* 971.4 and $[mc5+H_3O]^+$ at *m/z* 989.4, which are similar to the dissociation products observed for the $[CH_3(CH_2)_4NH_3•CB5]^+$ complex.

The $[CB5+H]^+$ product involves loss of neutral pentylamine ($CH_3(CH_2)_4NH_2$ *m/z* = 88.1) from the complex. The $[CB5+H_3O]^+$ cannot arise from direct dissociation; rather, it arises from reaction of $[CB5+H]^+$ product with H_2O. This is not unexpected; the hydronium complex is easily observed because adventitious H_2O exists in the trapping cell.

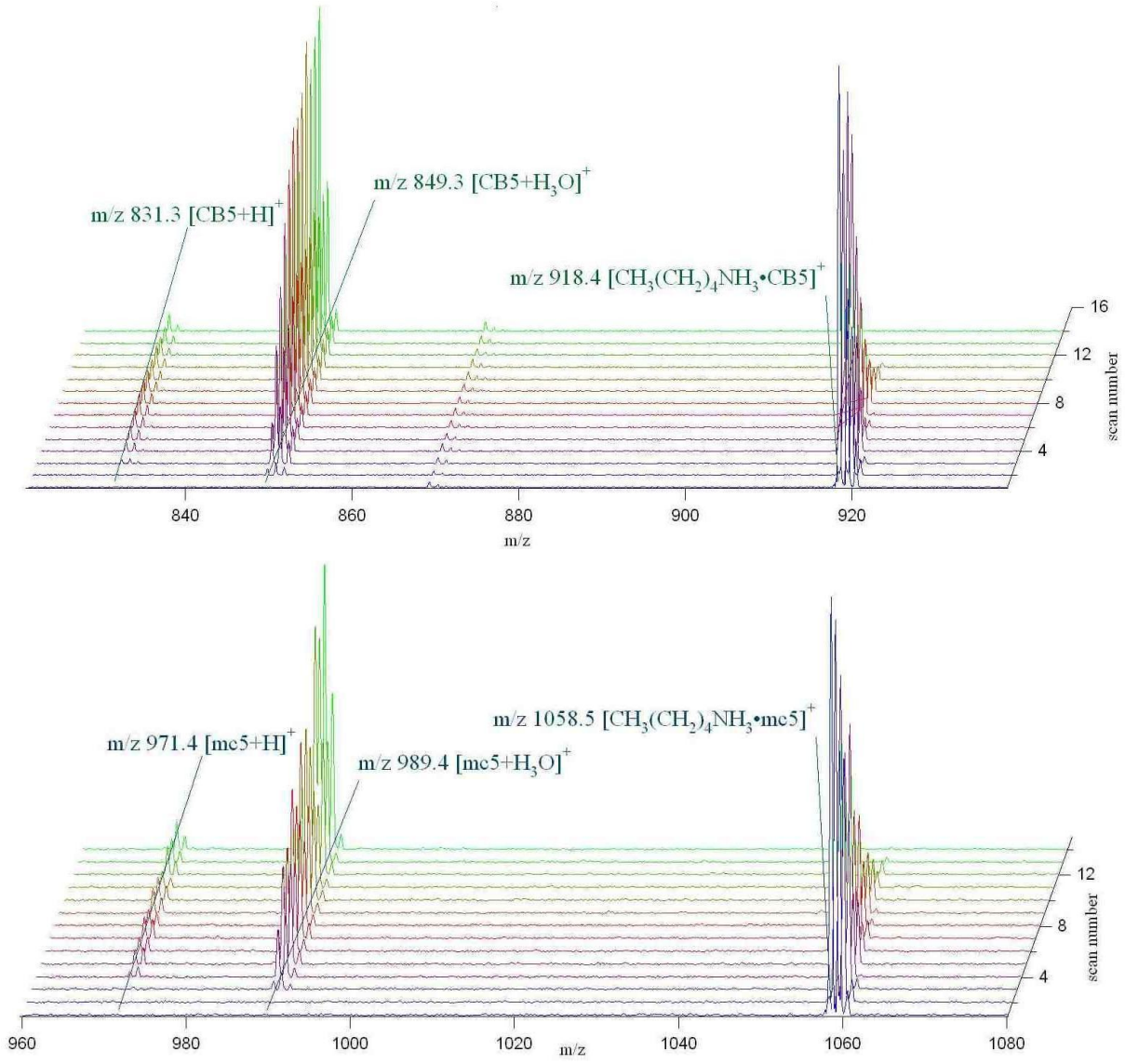

Figure 2.4. Set of $[CH_3(CH_2)_4NH_3•CB5]^+$ and $[CH_3(CH_2)_4NH_3•mc5]^+$ SORI-CID spectra with various SORI lengths (increasing scan numbers correspond to increasing SORI durations).

By varying the SORI length programmatically, the SORI energy added to the complex ions is varied. Thus a set of spectra with different dissociation ratios of the complex is obtained, shown in Figure 2.4, yielding semi-quantitative dissociation threshold information for $[CH_3(CH_2)_4NH_3•CB5]^+$ and $[CH_3(CH_2)_4NH_3•mc5]^+$.

Plotting the relative abundances of the product ions and parent ions against the SORI length gives us the SORI ion yield curves and disappearance curves. Figure 2.5 shows the SORI ion yield curves and disappearance curves for $[CH_3(CH_2)_4NH_3•CB5]^+$ and $[CH_3(CH_2)_4NH_3•mc5]^+$ from an average of two measurements.

It is evident that as the SORI length increases, the relative abundance of the parent ions, $[CH_3(CH_2)_4NH_3•CB5]^+$, decreases and the relative abundance of the product ions, $[CB5+H_3O]^+$ and $[CB5+H]^+$, increases. The same conclusions can be obtained for $[CH_3(CH_2)_4NH_3•mc5]^+$ from its ion yield and disappearance curves. The standard deviations of the points from two measurements are generally below 1×10^{-2}, thus error bars are not shown in these two graphs.

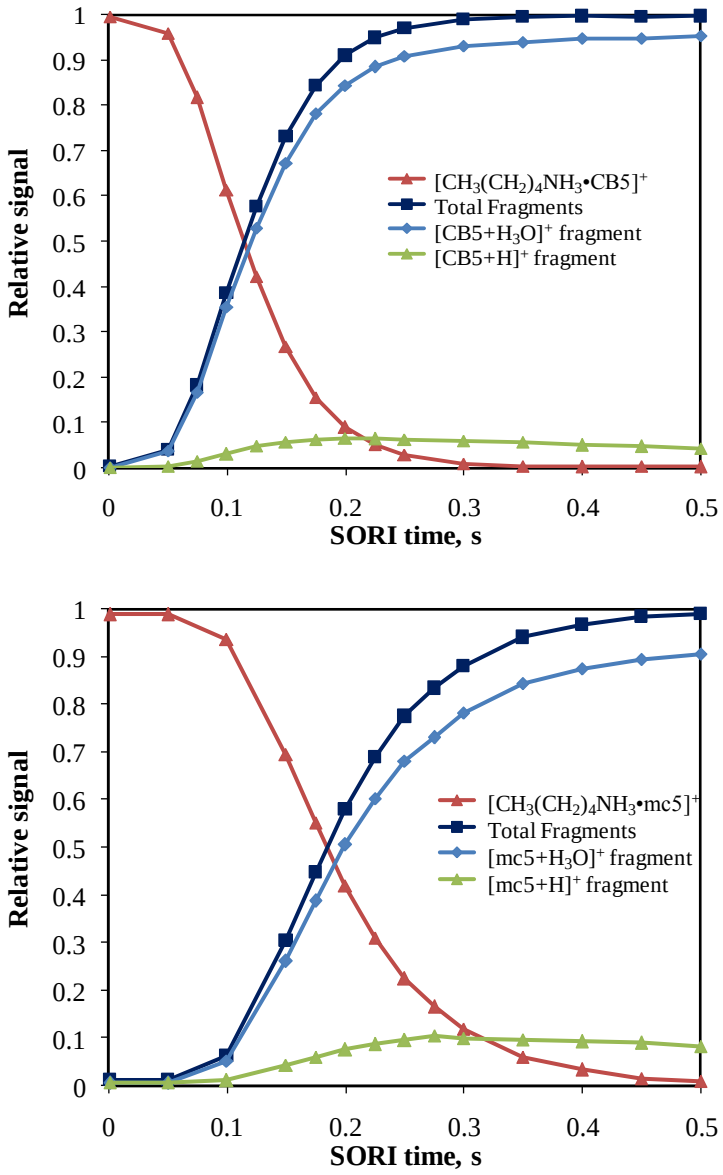

Figure 2.5. $[CH_3(CH_2)_4NH_3•CB5]^+$ and $[CH_3(CH_2)_4NH_3•mc5]^+$ SORI ion yield and disappearance curves.

Disappearance curves for $[CH_3(CH_2)_4NH_3•CB5]^+$ and $[CH_3(CH_2)_4NH_3•mc5]^+$ are extracted from Figure 2.5 and plotted together with other $[CH_3(CH_2)_nNH_3•CB5]^+$ and $[CH_3(CH_2)_nNH_3•mc5]^+$ complexes, as shown in Figure 2.6. The x-intercept has been changed

from SORI time to relative SORI energies, which can be determined by Eqn. (7) in chapter 1, for the purpose of easy comparison of complexes as *n* varies.

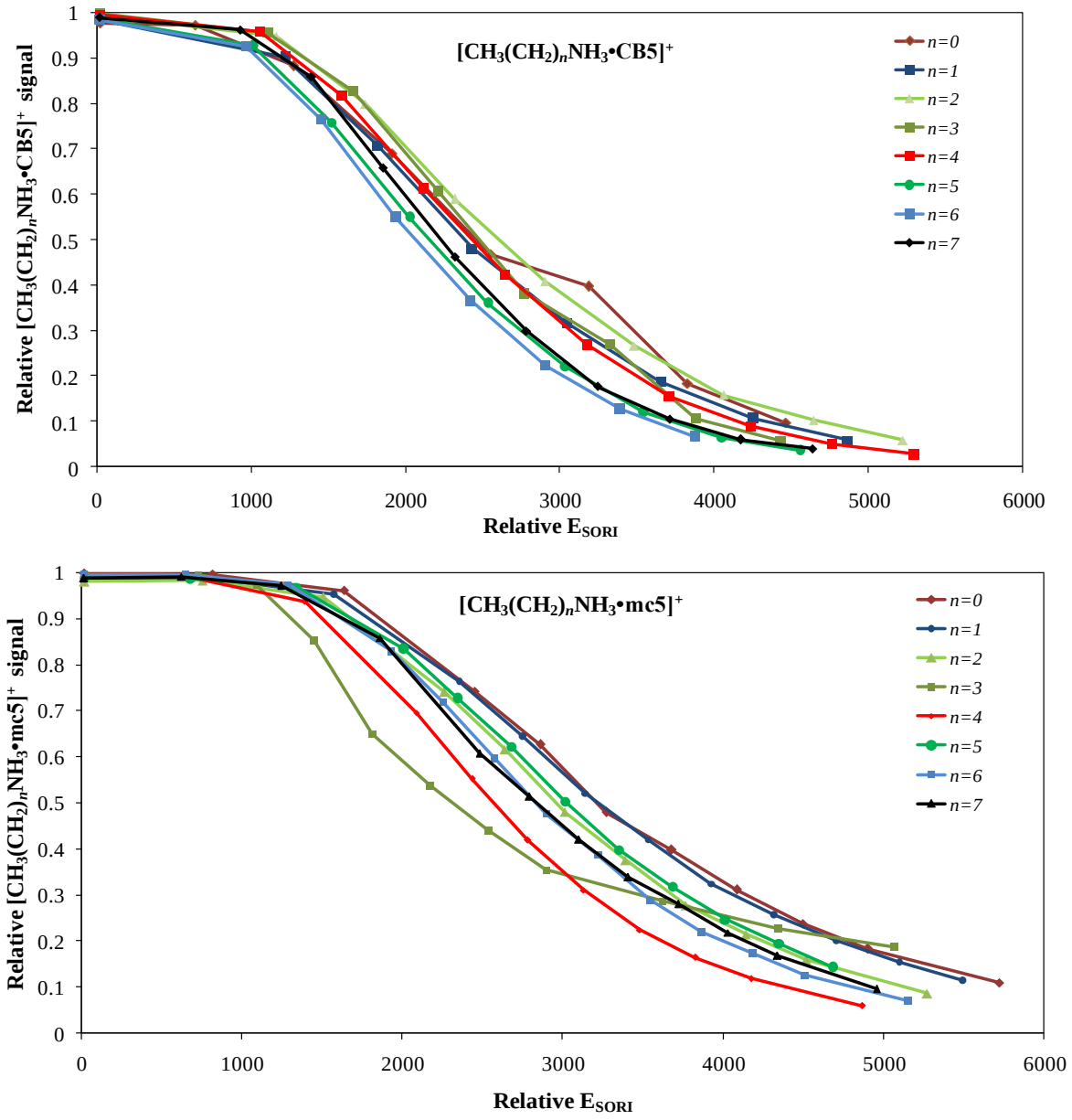

Figure 2.6. SORI disappearance curves for $[CH_3(CH_2)_nNH_3•CB5]^+$ and $[CH_3(CH_2)_nNH_3•mc5]^+$, n = 0-7.

Relative energies for 50% loss of the parent ion, $E_{SORI,50}$, are determined by linear fitting of the falling portion of each disappearance curve and calculation of the 50% loss point using the

fitted line. The energies for 50% loss of the parent ion ($E_{SORI,50}$) and standard errors are shown in Figure 2.7. Error bars represent standard errors from the linear fitting procedure used to derive the values.

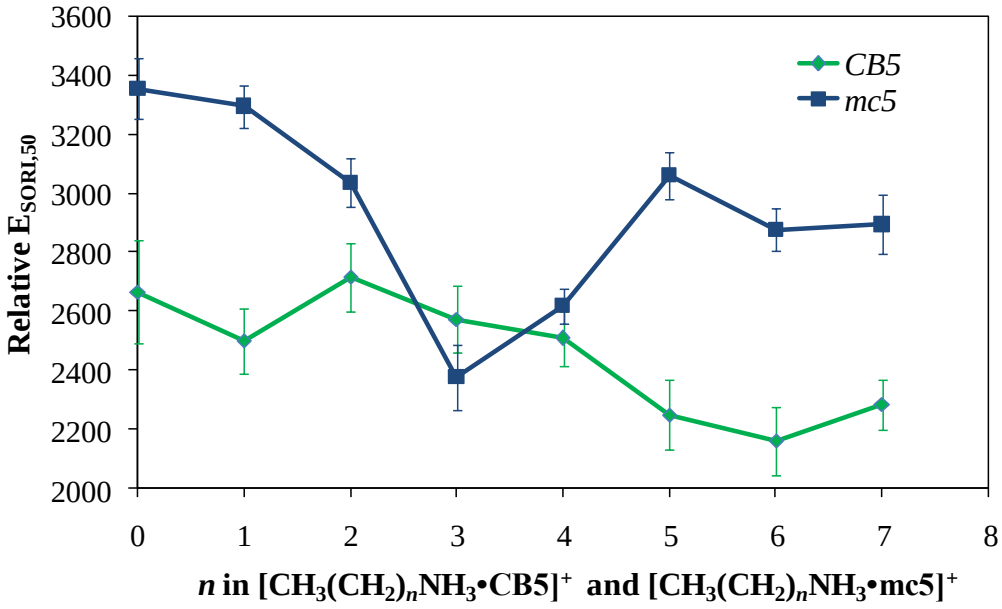

Figure 2.7. Relative SORI energies for 50% loss of $[CH_3(CH_2)_nNH_3•CB5]^+$ and $[CH_3(CH_2)_nNH_3•mc5]^+$ complexes, n = 0-7.

$E_{SORI,50}$ results for $[CH_3(CH_2)_nNH_3•CB5]^+$ and $[CH_3(CH_2)_nNH_3•mc5]^+$ are comparable since they are calculated using the same scaling. All of the $[CH_3(CH_2)_nNH_3•mc5]^+$ complexes except for $[CH_3(CH_2)_3NH_3•mc5]^+$ require higher collision energies than the corresponding $[CH_3(CH_2)_nNH_3•CB5]^+$ complexes. This phenomenon may due to the fact that the methyl groups along the equator of mc5 make it more rigid than CB5, although greater rigidity in the host will not necessarily lead to higher guest binding energies. But even if the binding energies are the same, the dissociation thresholds of $[CH_3(CH_2)_nNH_3•mc5]^+$ complexes should still be higher than

the corresponding $[CH_3(CH_2)_nNH_3•CB5]^+$ complexes. This is because the extra atoms in mc5 introduce additional vibrational states, increasing the density of states and slowing down dissociation relative to CB5.

Reactivity of $[CH_3(CH_2)_nNH_3•CB5]^+$ and $[CH_3(CH_2)_nNH_3•mc5]^+$ (n = 0-7).

Singly-charged ions of $[CH_3(CH_2)_nNH_3•CB5]^+$ (*m/z* range from 862.3 to 960.4) and $[CH_3(CH_2)_nNH_3•mc5]^+$ (*m/z* range from 1002.5 to 1100.6) were each isolated, then allowed to react with pairs of neutral amines in the trapping cell. Here solutions of CB5 with propylamine (n = 2) and butylamine (n = 3) are chosen to illustrate this experiment. Neutral propylamine and butylamine were introduced one after another into the ion-trapping region of the vacuum chamber and maintained at constant low partial pressures. $[CH_3(CH_2)_2NH_3•CB5]^+$ (*m/z* 890.3) ions are isolated and then allowed to exchange between this pair of primary neutral amines. This reaction is shown as the forward reaction below.

$$[CH_3(CH_2)_2NH_3•CB5]^+ + CH_3(CH_2)_3NH_2 \underset{k_r}{\overset{k_f}{\rightleftharpoons}} [CH_3(CH_2)_3NH_3•CB5]^+ + CH_3(CH_2)_2NH_2 \quad (1)$$

Then the isolation and exchange processes were repeated for $[CH_3(CH_2)_3NH_3•CB5]^+$ (*m/z* 904.3) ions with the same neutral pressures, which is shown as the reverse reaction in reaction (1). A relative abundance plot of $[CH_3(CH_2)_2NH_3•CB5]^+$ and $[CH_3(CH_2)_3NH_3•CB5]^+$ showing the process of reaction (1) from the forward and reverse directions is given in Figure 2.8.

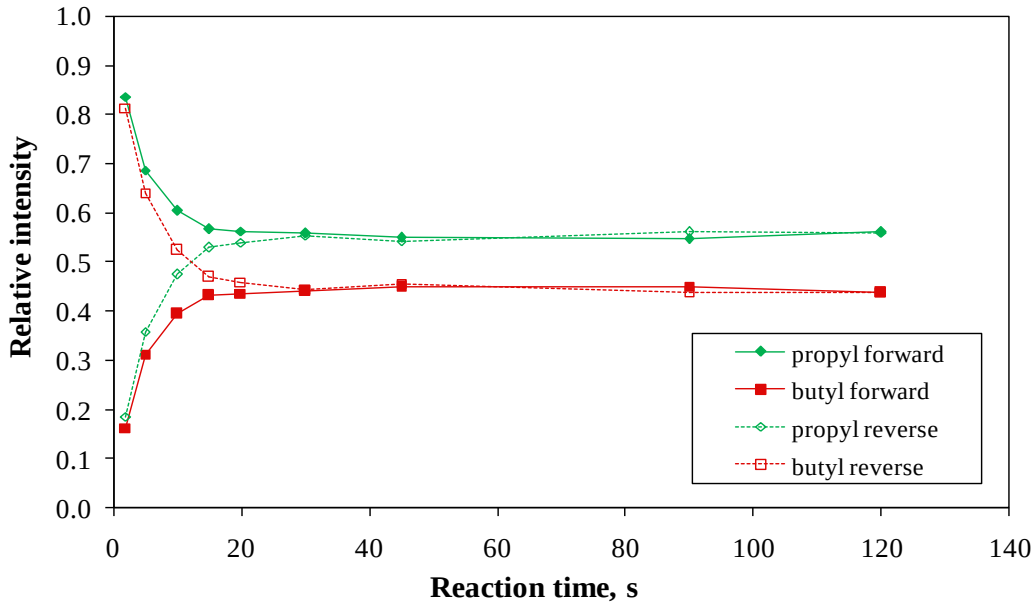

Figure 2.8. Relative abundances of the reactant and product ions.

The relative abundances of the reactant ions $[CH_3(CH_2)_2NH_3•CB5]^+$ and product ions $[CH_3(CH_2)_3NH_3•CB5]^+$ are extracted from a set of mass spectra collected by varying the reaction times. It is apparent that equilibrium has been achieved as the ratio of $[CH_3(CH_2)_2NH_3•CB5]^+$ to $[CH_3(CH_2)_3NH_3•CB5]^+$ becomes constant with time, and as the same ratios are obtained following transient ejection of either the reactant or the product ion from both directions. Measurements of the equilibrium constant for this reaction, K_{23}, were carried out three times in both the forward and reverse directions, and the results are compiled in Table 2.1. The standard Gibbs free energy change of reaction (1), ΔG^o_{23}, determined using Eqn. (12) in chapter 1, is -3.32 $\pm$ 0.96 kJ/mol.

Equilibrium constant	1 st	2 nd	3 rd	Average
$K_{forward}$	4.88	4.80	4.84	4.00 ± 1.31
$K_{reverse}$	2.27	2.35	4.87	

Table 2.1. Equilibrium constant of reaction (1) measured in the forward and reverse directions.

Another approach for determining the equilibrium constant is to measure the rate constants for this reaction. Rate constants are obtained by measuring the abundance of $[CH_3(CH_2)_2NH_3{\bullet}CB5]^+$ and $[CH_3(CH_2)_3NH_3{\bullet}CB5]^+$ ions as a function of time. This method is especially useful for the rapid determination of equilibrium constants for reactions that need a long time to reach equilibrium. Figure 2.9 shows the kinetic fit results for the relative abundance plot in Figure 2.8.

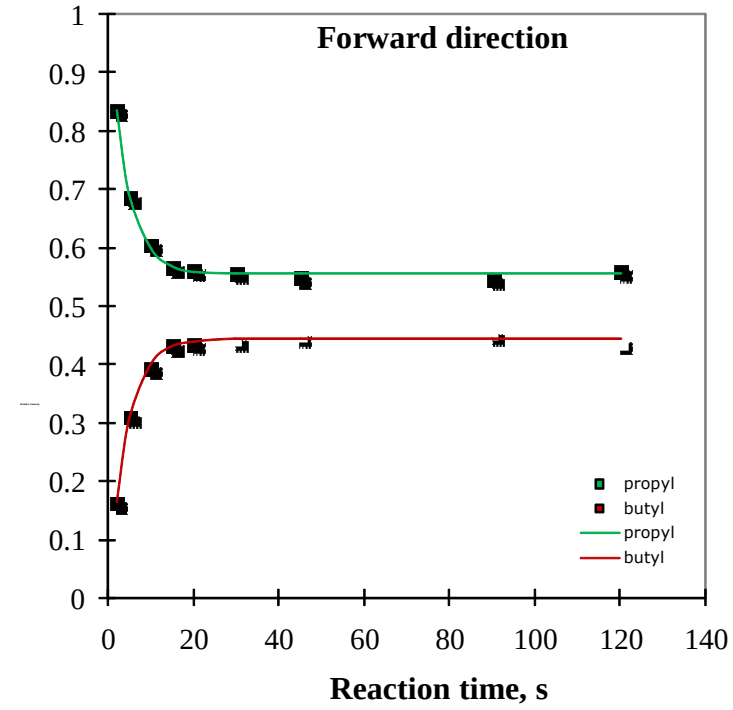

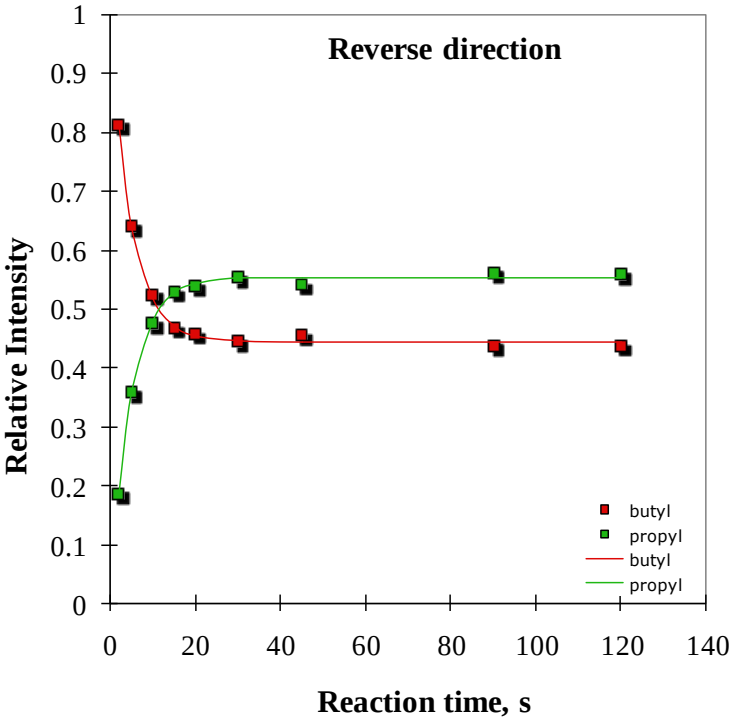

Figure 2.9. Kinetic fit results for the relative abundance plot.

Measurements in either the forward or the reverse direction were repeated three times. The rate constants and equilibrium constants extracted from the kinetic fit data of these relative abundance plots are compiled in Table 2.2.

Forward direction	1 st	2 nd	3 rd
k_f	2.91E-11	3.03E-11	2.77E-11
k_r	5.99E-12	6.33E-12	5.69E-12
K	4.87	4.78	4.86

Reverse direction	1 st	2 nd	3 rd
k_f	2.63E-11	2.64E-11	2.51E-11
k_r	1.16E-11	1.14E-11	5.14E-12
K	2.26	2.32	4.88

Table 2.2. Rate constants (cm^3 $molecule^{-1}$ s^{-1}) and equilibrium constants of reaction (1) from kinetic fit data.

The equilibrium constant K_{23} and standard Gibbs free energy change ΔG^o_{23} derived from the kinetic fit method are 4.00 $\pm$1.32 and -3.31 $\pm$0.97 kJ/mol respectively, showing good agreement with the results from the equilibrium ratio method. ΔG^o_{23} can also be expressed as the free energy difference between products and reactants in reaction (1), as shown in Eqn. (2), in which ΔG^o_f means the standard free energy of formation.

$$\Delta G^o_{23} = \{\Delta G^o_{f\,CH_3(CH_2)_2NH_2} + \Delta G^o_{f\,[CH_3(CH_2)_3NH_3\bullet CB5]^+}\} - \{\Delta G^o_{f\,CH_3(CH_2)_3NH_2} + \Delta G^o_{f\,[CH_3(CH_2)_2NH_3\bullet CB5]^+}\} \qquad (2)$$

As the alkyl chain length increases, ΔG_f^o for the n-alkylmonoamines becomes increasingly negative, which means $CH_3(CH_2)_2NH_2$ has a more positive ΔG_f^o than that of $CH_3(CH_2)_3NH_2$. Therefore, the first term minus the third term in Eqn. (2) will give a positive value. Since ΔG_{23}^o is negative according to our experiment, it is evident that the second term is more negative than the fourth term in Eqn. (2). Thus we can conclude that $[CH_3(CH_2)_3NH_3 \bullet CB5]^+$ complex has a more negative ΔG_f^o than $[CH_3(CH_2)_2NH_3 \bullet CB5]^+$, which means $[CH_3(CH_2)_3NH_3 \bullet CB5]^+$ is more stable than $[CH_3(CH_2)_2NH_3 \bullet CB5]^+$.

The exchange reactions of primary alkylmonoamines on protonated CB5 as well as protonated mc5 were measured for propylamine through octylamine. The free energy changes of all these reactions are listed in Table 2.3.

ΔG°	ΔG°_{23}	ΔG°_{34}	ΔG°_{45}	ΔG°_{56}	ΔG°_{67}
CB5	-3.32 ±0.96	-0.72 ±0.07	-0.72 ±0.11	-1.02 ±0.17	1.56 ±0.38
mc5	-1.50 ±0.55	-0.70 ±0.11	-0.51 ±0.12	2.72 ±1.44	2.63 ±0.16

Table 2.3. Standard free energy changes for exchange reactions on protonated CB5 and protonated mc5.

All of the exchange reactions on $[CH_3(CH_2)_nNH_3 \bullet CB5]^+$ have negative ΔG° values except for ΔG_{67}^o, whereas the reactions on $[CH_3(CH_2)_nNH_3 \bullet mc5]^+$ have negative ΔG° values except for ΔG_{56}^o and ΔG_{67}^o. We conclude from the negative ΔG_{23}^o that $[CH_3(CH_2)_3NH_3 \bullet CB5]^+$ is more stable than $[CH_3(CH_2)_2NH_3 \bullet CB5]^+$ as noted above. The extension of Eqn. (2) to the other exchange reactions on protonated CB5 and protonated mc5 will easily give such a conclusion: generally, the $[CH_3(CH_2)_nNH_3 \bullet CB5]^+$ complexes become increasingly stable as *n* increases from

2 to 6, and $[CH_3(CH_2)_nNH_3 \bullet mc5]^+$ complex also becomes increasingly stable as *n* increases from 2 to 5.

Taking reaction (1) for instance, the exchange reactions on $[CH_3(CH_2)_2NH_3 \bullet CB5]^+$ involve breaking bonds to $CH_3(CH_2)_2NH_2$ and formation of bonds with $CH_3(CH_2)_3NH_2$. Therefore, the standard free energy change ΔG_{23}^o also reflects the binding affinities of protonated CB5 for propylamine and butylamine. If we assume the binding affinity of protonated CB5 for propylamine is zero, the relative binding affinity sequence can be easily determined from the standard free energy changes. Figure 2.10 shows the relative binding affinities of protonated CB5 and protonated mc5 for $CH_3(CH_2)_nNH_2$. The highest binding affinity appears at $n = 6$ for protonated CB5 and $n = 5$ for protonated mc5, which means $n = 6$ is the most stable complex measured for $[CH_3(CH_2)_nNH_3 \bullet CB5]^+$ and $n = 5$ is the most stable for $[CH_3(CH_2)_nNH_3 \bullet mc5]^+$. This is reasonable given that CB5 is more flexible, and therefore can accommodate a larger guest, than mc5.

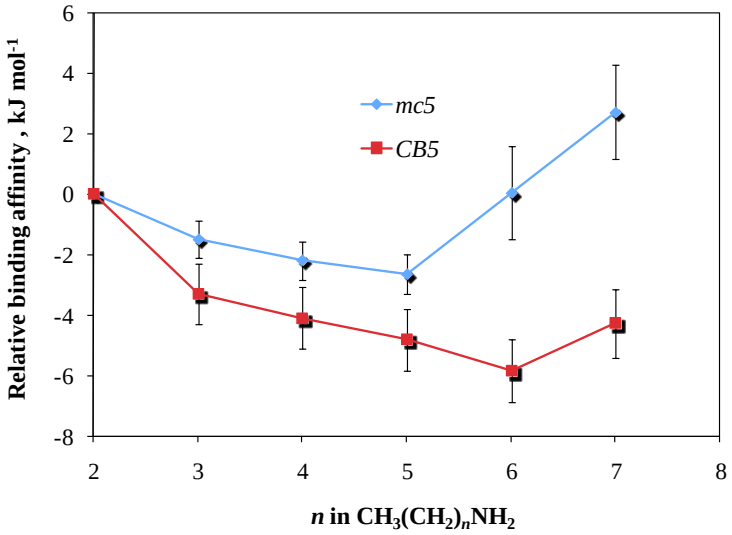

Figure 2.10. The relative binding affinities of protonated CB5 and protonated mc5 for $CH_3(CH_2)_nNH_2$.

Computational Results.

Binding energies of the complexes can be derived from the computed energies of their components. Experimentally we observe all $[CH_3(CH_2)_nNH_3 \bullet CB5]^+$ complexes dissociate into neutral monoamine and singly protonated CB5. Although hydronium CB5 product is also observed in SORI event, it comes from the binding of protonated CB5 with H_2O. Therefore, the binding energy of $[CH_3(CH_2)_nNH_3 \bullet CB5]^+$ complex can be modeled by calculating the energy change for binding neutral monoamine to singly protonated CB5. The computed binding energies for $[CH_3(CH_2)_nNH_3 \bullet CB5]^+$, derived from B3LYP/6-31+G* geometry optimizations, are given in Table 2.4.

N	$[CH_3(CH_2)_nNH_3 \bullet CB5]^+$
0	-242.3390
1	-243.2062
2	-243.9277
3	-244.7384
4	-242.3429
5	-242.1067
6	-241.7233
7	-233.9635

Table 2.4. Computed enthalpy changes (kJ/mol) for binding neutral monoamine to singly protonated CB5.

Therefore, the dissociation energies can be determined directly for $[CH_3(CH_2)_nNH_3 \bullet CB5]^+$ from their computed binding energies. Figure 2.11 shows the computed dissociation energies for $[CH_3(CH_2)_nNH_3 \bullet CB5]^+$.

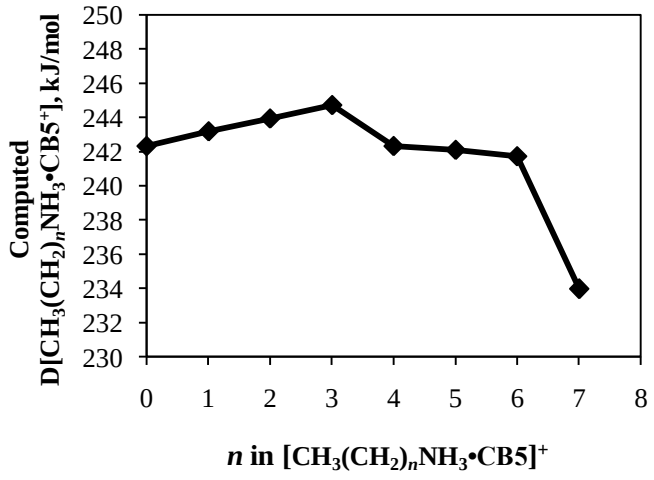

Figure 2.11. Computed dissociation energies for $[CH_3(CH_2)_nNH_3 \bullet CB5]^+$.

Energy changes of the reactions on $[CH_3(CH_2)_nNH_3 \bullet CB5]^+$ can also be computed. For the exchange reaction of $CH_3(CH_2)_nNH_2$ for $CH_3(CH_2)_{n+1}NH_2$ on $[CH_3(CH_2)_nNH_3 \bullet CB5]^+$, the computed energies of products, $[CH_3(CH_2)_{n+1}NH_3 \bullet CB5]^+$ and $CH_3(CH_2)_nNH_2$, subtracted by the computed energies of reactants, $[CH_3(CH_2)_nNH_3 \bullet CB5]^+$ and $CH_3(CH_2)_{n+1}NH_2$, would give us the computed energy change of the reaction. Table 2.5 shows the computed energy changes for the exchange reactions on CB5.

Computed ΔE (kJ/mol)	ΔE_{23}	ΔE_{34}	ΔE_{45}	ΔE_{56}	ΔE_{67}
CB5	-0.81	2.40	0.24	0.38	7.76

Table 2.5. Computed energy changes for exchange reactions on CB5.

Discussion

Distinguishing the conformational structures of the complexes.

The experimental and computational results presented above are consistent with external binding of alkylammonium by CB5 and mc5 in the gas phase. The most straightforward evidence is from their reactivities with neutral alkylmonoamines. The caged guest is difficult to displace, whereas externally bound amines are easily exchanged.[8] Internal complexes need more collisions with neutral gas molecules to cause the displacement of guest, thus they require longer reaction times to reach equilibrium. All of the exchange reactions on $[CH_3(CH_2)_nNH_3 \bullet CB5]^+$ reach equilibrium quickly, supporting the external binding of alkylammonium with CB5. Although the exchange reactions on $[CH_3(CH_2)_nNH_3 \bullet mc5]^+$ are slightly slower than the

corresponding $[CH_3(CH_2)_nNH_3 \bullet CB5]^+$, they are still fast enough to support the external binding of alkylammonium with mc5.

The experimentally observed dissociation behavior also provides direct evidence in support of external binding. If $[CH_3(CH_2)_nNH_3 \bullet CB5]^+$ and $[CH_3(CH_2)_nNH_3 \bullet mc5]^+$ are internally-bound complexes, we would expect they need higher SORI energy to induce dissociation compared to externally-bound complexes, which do not require removal of the guest from the interior of the cage. Further, if the complexes were internal we would expect to observe lots of cage fragments of CB5 or mc5 in their SORI spectra, since loss of the amine is competitive with covalent bond breaking of the CB5 or mc5 cage. However, we observe that complexes of $[CH_3(CH_2)_nNH_3 \bullet CB5]^+$ and $[CH_3(CH_2)_nNH_3 \bullet mc5]^+$ are all easily dissociated via loss of the neutral amine when relatively low SORI energies are applied. The SORI amplitude for the dissociation of CB5 or mc5 complexes is 38.5 V, which is relatively smaller than that of the CB6 complexes, which are believed to be internal (see Chapter 3). Additionally, the SORI spectra of these complexes lack any evident peaks showing the existence of cage fragments of CB5 or mc5.

The results of B3LYP/6-31+G* computational studies are in agreement with the experimental results. At this level of theory, the external binding complexes of $[CH_3(CH_2)_nNH_3 \bullet CB5]^+$ and $[CH_3(CH_2)_nNH_3 \bullet mc5]^+$ are lower in energy than the corresponding internally-bound complexes.

Dissociation energies of $[CH_3(CH_2)_nNH_3 \bullet CB5]^+$ and $[CH_3(CH_2)_nNH_3 \bullet mc5]^+$.

For the complexes formed by cucurbituril with alkylmonoammonium ions, two general factors can affect the stability of the complex. One is the conformation of the complex, and the other is the hydrogen bond strength between the ammonium ion and the carbonyl dipoles. All of the $[CH_3(CH_2)_nNH_3 \bullet CB5]^+$ and $[CH_3(CH_2)_nNH_3 \bullet mc5]^+$ are externally-bound complexes.

Therefore, their stabilities and dissociation energies are mainly determined by the hydrogen bonding interactions. Not surprisingly, all the experimental stabilities fall within a narrow range, with differences likely due to noncovalent interactions between the alkyl tails of the guests and the cucurbituril host.

The experimental (Figure 2.7) and computational (Figure 2.11) dissociation energy trends of $[CH_3(CH_2)_nNH_3 \bullet CB5]^+$ are quite similar, reaching a maximum at intermediate size of ammonium ions. This trend can be explained by the strength of the tripodal hydrogen bond, N-H ··O=C, formed by the carbonyl portal of the cucurbituril with the ammonium ion. As the alkyl chain length increases, the inductive effect of the alkyl group on $–NH_3^+$ becomes stronger and the electron cloud density of N becomes larger, so that the N-H bond gets more stable and requires more energy to break. Although the basicity of ammonium ion increases with increasing alkyl chain length, which would lead to increased hydrogen bonding, this increase in basicity with chain length becomes negligible once the chain reaches a certain length. For $n > 2$ complexes, the bending of the alkyl chains may result in the terminal ammonium binding asymmetrically to the carbonyl portal of CB5. Mechanistically, it is possible that one of the N-H bonds is more easily broken than the other two, shifting the position of the transition state and lowering the activation energy, supplying a plausible explanation for this trend. In addition, there is an entropic cost to binding the larger systems, which gets greater as chain length increases. The $n = 1$ and $n = 7$ complexes fit in this trend within experimental error.

The experiments show the dissociation threshold of $[CH_3(CH_2)_nNH_3 \bullet CB5]^+$ is greatest for $n = 2$ complex, whereas the computed results suggest that the lowest energy complex appears when $n = 3$. The difference between computed dissociation energy and the experimental threshold data can be explained by the features of the two approaches in probing the dissociation energy. The

computed dissociation energy is obtained from the energy difference between a fully relaxed complex and fully relaxed products. The experimental threshold data reflects the activation barriers for the dissociation of complex, which will be the same as the computed dissociation energy only when the reaction has no reverse activation barrier. The dissociation of $[CH_3(CH_2)_nNH_3 \bullet CB5]^+$ is certainly not such a barrier-free reaction. Therefore, the disagreement between the computational and experimental results is not unexpected. Computational methods for determining the top of the activation barrier require calculation of the potential surface along the dissociation channel, which would be quite challenging for systems as large as those studied here.

Free energy changes.

As Figure 2.12 shows, the experimentally obtained free energy changes for $[CH_3(CH_2)_nNH_3 \bullet CB5]^+$ have similar trends as *n* increases as the computed energy changes.

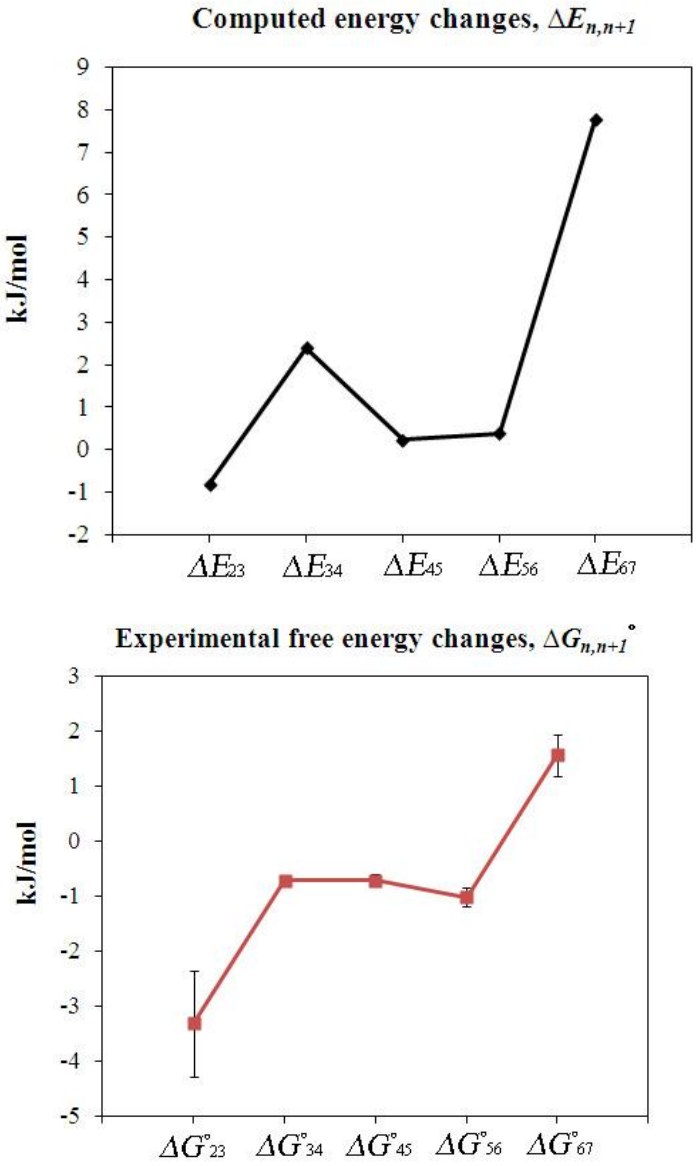

Figure 2.12. Computed energy changes and experimental free energy changes for the exchange reactions on CB5.

The similarity in the overall trends of the two curves is remarkable. Although the experimental free energy change values are quite different from the corresponding computed values, it is notable that all the computed values are 2-5 kJ/mol more than the experimental values. A reasonable explanation is that a systematic error exists in either the calculations or the

experiments. For the level of theory we used in this thesis, this difference is quite negligible since the theoretical calculations cannot be accurate to better than about 5 kJ/mol in any event.

Conclusions

Reactivity measurements for the complexes formed by CB5 or mc5 with alkylmonoammonium ions and observation of their collision-induced fragmentation patterns both confirm the externally-bound conformation of the complexes in the gas phase. These results suggest that SORI-CID and reactivity tests can be used to identify molecule structures for gas-phase ions. Energy-resolved SORI-CID gives the overall dissociation energy trends for CB5 or mc5 complexes and the optimum alkylammonium chain length for binding CB5 or mc5 in the gas phase. The measurement of rate and equilibrium constants for CB5 or mc5 molecular systems displays their reactivities at low pressure. This study is valuable for the measurement of fundamental thermochemical quantities such as energy changes in chemical reactions of supramolecules, complementing results obtained from high pressure and condensed-phase conditions. B3LYP/6-31+G* computational studies are generally consistent with the experiments and provide valuable complementary information to the experimental work. This investigation offers potentially powerful new analytical tools that might enable the determination of molecular conformation, reactivity, etc.

References

(1) Zhao, J.; Kim, H.-J.; Oh, J.; Kim, S.-Y.; Lee, J. W.; Sakamoto, S.; Yamaguchi, K.; Kim, K.

Angew. Chem. Int. Ed. **2001**, *40*, 4233-4235

(2) Lee, J. W.; Samal, S.; Selvapalam, N.; Kim, H.-J.; Kim, K. *Acc. Chem. Res.* **2003**, *36*, 621-630.

(3) Jon, S. Y.; Selvapalam, N.; Oh, D. H.; Kang, J.-K.; Kim, S.-Y.; Jeon, Y. J.; Lee, J. W.; Kim, K. *J. Am. Chem. Soc.* **2003**, *125*, 10186-10187.

(4) Kellersberger, K. A.; Anderson, J. D.; Ward, S. M.; Krakowiak, K. E.; Dearden, D. V. *J. Am. Chem. Soc.* **2001**, *123*, 11316-11317.

(5) Zhang, H.; Dearden, D. V. *Chem. Commun.* in preparation.

(6) El Haouaj, M.; Luhmer, M.; Ko, Y. H.; Kim, K.; Bartik, K. *J. Chem. Soc. Perkin Trans. 2* **2001**, 804-807.

(7) Jansen, K.; Buschmann, H.-J.; Wego, A.; Döpp, D.; Mayer, C.; Drexler, H.-J.; Holdt, H.-J.; Schollmeyer, E. *J. Inclusion Phenom. Macrocyclic Chem.* **2001**, *39*, 357-363.

(8) Zhang, H.; Paulsen, E. S.; Walker, K. A.; Krakowiak, K. E.; Dearden, D. V. *J. Am. Chem. Soc*. **2003**, *125*, 9284-9285.

(9) Dearden, D.V.; Dejsupa, C.; Liang, Y.; Bradshaw, J. S.; Izatt, R. M. *J. Am. Chem. Soc*. **1997**, *119*, 353-359.

(10) Senko, M. W.; Canterbury, J. D.; Guan, S.; Marshall, A. G. *Rapid Commun. Mass Spectrom.* **1996**, *10*, 1839-1844.

(11) http://www.wavemetrics.com/.

(12) Kim, J.; Jung, I.-S.; Kim, S.-Y.; Lee, E.; Kang, J.-k.;Sakamoto, S.; Yamaguchi, K.; Kim,K. *J. Am. Chem. Soc*. **2000**, *122*, 540-541.

(13) Flinn, A.; Hough, G. C.; Stoddart, J. F.; Williams, D. J. *Angew. Chem. Int. Ed. Engl.* **1992**, *31*, 1475-1477.

(14) Bakhtiar, R.; Holznagel, C. M.; Jacobson, D. B. *Organometallics* **1993**, *12*, 621-623.

(15) Chen, L.; Wang, T.-C. L.; Ricca, T. L.; Marshall, A. G. *Anal. Chem.* **1987**, *59*, 449-454.

(16) Jiao, C. Q.; Ranatunga, D. R. A.; Vaughn, W. E.; Freiser, B. S. *J. Am. Soc. Mass Spectrom.* **1996**, *7*, 118-122.

(17) Bartmess, J. E.; Georgiadis, R. M. *Vacuum* **1983**, *33*, 149-153.

(18) Halgren, T. A. *J. Comput. Chem.* **1996**, *17*, 490-519.

(19) Black, G.; Didier,B.; Feller, D.; Gracio, D.; Hackler, M.; Havre, S.; Jones, D.; Jurrus, E.; Keller, T.; Lansing, C.; Matsumoto, S.; Palmer, B.; Peterson, M.; Schuchardt, K.; Stephan, E.; Taylor, H.; Thomas, G.; Vorpagel, E.; Windus, T.; Winters, C. *Ecce*; Pacific Northwest National Laboratory: Richland, Washington, USA, 2003.

(20) Apra, E. W., T. L.; Straatsma, T. P.; Bylaska, E. J.; de Jong, W.; Hirata, S.; Valiev, M.; Hackler, M. T.; Pollack, L.; Kowalski, K.; Harrison, R. J.; Dupuis, M.; Smith, D. M. A.; Nieplocha, J.; Tipparaju, V.; Krishnan, M.; Auer, A. A.; Brown, E.; Cisneros, G.; Fann, G. I.; Fruchtl, H.; Garza, J.; Hirao, K.; Kendall, R.; Nichols, J. A.; Tsemekhman, K.; Wolinski, K.; Anchell, J.; Bernholdt, D.; Borowski, P.; Clark, T.; Clerc, D.; Dachsel, H.; Deegan, M.; Dyall, K.; Elwood, D.; Glendening, E.; Gutowski, M.; Hess, A.; Jaffe, J.; Johnson, B.; Ju, J.; Kobayashi, R.; Kutteh, R.; Lin, Z.; Littlefield, R.; Long, X.; Meng, B.; Nakajima, T.; Niu, S.; Rosing, M.; Sandrone, G.; Stave, M.; Taylor, H.; Thomas, G.; van Lenthe, J.; Wong, A.; Zhang, Z.; 4.7 ed.; Pacific Northwest National Laboratory: Richland, Washington 99352-0999, USA, 2005.

(21) Oh, K. S.; Yoon, J.; Kim, K. S. *J. Phys. Chem*. B **2001**, *105*, 9726-9731.

Chapter 3

Characterization of cucurbit[n]uril complexes with alkylmonoammonium ions in the gas phase via experiment and theory (n = 6, 7)

Introduction

Cucurbit[6]uril[1] (abbreviated CB6, Figure 3.1) has been known for over 100 years and is the most well known molecule in the cucurbituril family. It has a hydrophobic cavity with an interior volume of 163 Å^3, and two carbonyl-lined portals with diameters of 3.9 Å.[2] With approximately the proper size to accommodate alkyldiammonium cations[3] and other species[4,5] within its interior cavity in solution, CB6 is known to serve as the "wheel" component of rotaxane structures in condensed media.

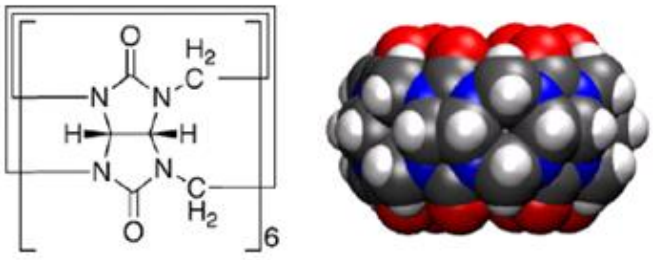

Figure 3.1. Left: structural formula for cucurbit[6]uril. Right: cucurbit[6]uril model (gray = carbon, red = oxygen, blue = nitrogen, white = hydrogen).

Rotaxanes are supramolecular assemblies that involve a wheel-and-axle architecture with a linear molecule (the "axle") threaded through another cyclic species (the "wheel"). Bulky groups at the ends of the axle prevent the wheel molecule from slipping off. Pseudorotaxanes have a similar architecture but lack the bulky stopping groups. The complexes formed by CB6 with

alkyldiammonium cations in solution have pseudorotaxane structures,[3] where the diammonium chain is threaded through the cucurbituril. Zhang et al.[6] have found that these pseudorotaxane complexes can survive into the gas phase and exhibit dissociation and reactivity properties distinct from those of nonrotaxanes. Briefly, collisional activation and dissociation of the internal pseudorotaxane complexes is relatively difficult, whereas corresponding non-threaded external complexes dissociate with low-energy collisional activation via simple loss of the amine. Additionally, pseudorotaxane complexes react with neutral amines via slow addition, whereas non-threaded external complexes react via rapid amine exchange.

Mass spectrometry remains one of the key tools in the study of molecular recognition in the gas phase. Among mass spectrometric methods, Fourier transform ion cyclotron resonance mass spectrometry (FTICR/MS) has the unique ability of trapping ions for extended periods, which allows for long time scale measurements of ion-molecule equilibrium reactions.

The goal of this chapter is to characterize the structures of complexes formed by CB6 or CB7 with alkylmonoammonium ions in the gas phase. In the work of Mock and coworkers, the host-guest chemistry between CB6 and alkylammonium was investigated in solution using NMR or UV techniques.[3] Due to hydrophobic interactions and charge-dipole attractions, CB6 forms pseudorotaxane complexes with alkylammonium ions. Of the primary monoammonium complexes of CB6 examined, the butylammonium complex was the most stable in solution. Will the CB6 pseudorotaxanes be observed in the gas phase where the entropic driving force of releasing solvent, believed to be responsible for their stability in solution, is not present? Will the butyl substituent remain the most stable one for homologues in the gas phase? What about host molecules with larger portal and cavity sizes, such as CB7? Will it also form pseudorotaxanes with alkylammonium like those of CB6? Here we will investigate the collision-induced

dissociation behavior of these complexes and their reactivity with neutral amines. In addition, these studies are complemented by high-level computational modeling of the same systems.

Experimental Section

ESI mass spectrometry. Collision-induced dissociation experiments were carried out using a Fourier transform ion cyclotron resonance mass spectrometer[7] (model APEX 47e; Bruker Daltonics; Billerica, MA) equipped with a 4.7 Tesla superconducting magnet. This instrument was controlled by a MIDAS data system,[8] and experimental data were processed using the Igor program (version 6.04; WaveMetrics; Lake Oswego, OR). Reactivity experiments were carried out on a 9.4 Tesla FT ICR mass spectrometer (model APEX II; Bruker Daltonics; Billerica, MA). An XMASS data system (version 6.0.2; Bruker Daltonics) was used to control this instrument and perform the data analysis. The electrospray ionization source was typically operated at a flow rate of 30 μL h^{-1}, and the spray needle was typically biased at +1.5 kV. These values were adjusted for optimum electrospray signal amplitude and stability.

Materials and sample preparation. Cucurbit[6]uril, cucurbit[7]uril and alkylmonoamines were purchased from Sigma Chemical Co. (St. Louis MO). All were used as purchased without additional purification. Alkylmonoamines were dissolved in pure methanol to a concentration of 5×10^{-4} M. CB6 stock solution was prepared by dissolving solid samples in a 70:30 formic acid/methanol mixture to a concentration of 2×10^{-4} M. CB7 was dissolved in 50:50 water/methanol solvent to the same concentration as CB6 without using acid. Electrospray solutions were prepared by mixing 100 μL of the CB6 or CB7 stock solution with 100 μL of the

n-alkylmonoamine solution, then diluting to 1 mL total volume with 50:50 water/methanol solvent. The final concentration of CB6 or CB7 analyte was 20 μM in the electrospray solutions.

SORI CID Experiments. Collision-induced dissociation (CID) was conducted using the sustained off-resonance irradiation (SORI) method.[9] Stored waveform inverse Fourier transform (SWIFT) techniques[10] were used to isolate ions of interest. Isolation was followed by introducing argon as a collision gas. Ar was introduced using a Freiser-type pulsed leak valve[11] with a backing pressure of 30 psig maintaining during the experiment. In the SORI events, the gas pulsed-valve was activated for 6 ms, yielding an Ar background pressure in the trapping cell of about 1×10^{-5} mbar. Single-frequency 1 kHz off-resonance irradiation was applied to the target ions during the gas pulse. The length of the off-resonance irradiation event was varied systematically from 1 ms to 500 ms, with the amplitude maintained at 49.5 V_{pp} (measured at the vacuum feedthrough to the trapping cell). The duration of the SORI events depended on the length of the off-resonance irradiation. Following the SORI event was a 10 s delay to allow the instrument to return to base pressure (10^{-9} mbar) prior to broadband excitation and detection. Six scans were averaged for each SORI duration.

Reactivity experiments. The reactivities of the CB6 and CB7 complex ions with neutral alkylmonoamines were studied on a 9.4 Tesla FT ICR mass spectrometer. A solution of CB6 or CB7 with one of the alkylmonoamines was electrosprayed to produce the CB6 or CB7 complex ions, which were then isolated and trapped in the FTICR cell containing a constant pressure of a pair of neutral amines (~10^{-7} mbar total). The partial pressure of each neutral alkylmonoamine was measured using a Stabil-Ion gauge. Exchange of the two amines on the protonated CB6 or CB7 was allowed to proceed to equilibrium. The reaction time (between isolation of the ionic reactant and detection of reactants and products) was varied programmatically and the mass

spectra were recorded using the XMASS program. Following this measurement, the ion source was flushed and then the solution of CB6 or CB7 with the other alkylmonoamine was electrosprayed. The measurement of the equilibrium constant was again performed with the same neutral pressures. Three measurements were conducted for each complex.

Computational methods. The structures of the complexes were sketched using the Maestro/MacroModel modeling package (Macromodel version 7.1; Schrödinger, Inc.; Portland, OR). Conformational searches were carried out using the MMFF94S force field[12] with no nonbonded cutoffs and employing the MCMM method with automatic setup. The lowest-energy structures found in the conformational searches were used as the starting point for B3LYP/6-31+G* geometry optimization. All of these calculations were performed by Dr. Dearden using the ECCE package[13] (version 3.1; Pacific Northwest National Laboratory; Richland, WA), and used the computational engine of NWChem[14] (version 4.7; Pacific Northwest National Laboratory; Richland, WA).

Results and Discussion

Characterization of CB6 complexes.

Solutions of CB6+$CH_3(CH_2)_nNH_2$ (n = 0-8) were each electrosprayed into the 4.7 T FTICR mass spectrometer. The ESI mass spectra are dominated by a single peak corresponding to the singly-charged ions $[CH_3(CH_2)_nNH_3@CB6]^+$ (*m/z* range from 1028.3 to 1140.5). Here, following the notation of Smalley,[15] the "@" symbol indicates inclusion of the species. We will describe the evidence for it being represented as an inclusion complex later.

$[CH_3(CH_2)_nNH_3@CB6]^+$ ions were first isolated using SWIFT and then excited 1 kHz below their resonant frequency. This excitation results in energy being gradually added to the $[CH_3(CH_2)_nNH_3@CB6]^+$ ions through mild collisions so that the lowest energy dissociation channels can be selected. By varying the collision time systematically, we obtain a set of mass spectra with different amounts of collisional excitation, and therefore different degrees of dissociation of the $[CH_3(CH_2)_nNH_3@CB6]^+$ complex. Plotting the relative abundance of the product ions and parent ions vs. the SORI length gives us the SORI ion yield curves and parent disappearance curve. Here the SORI ion yield curves and disappearance curve for $[CH_3(CH_2)_2NH_3@CB6]^+$ are given as an example, shown in Figure 3.2.

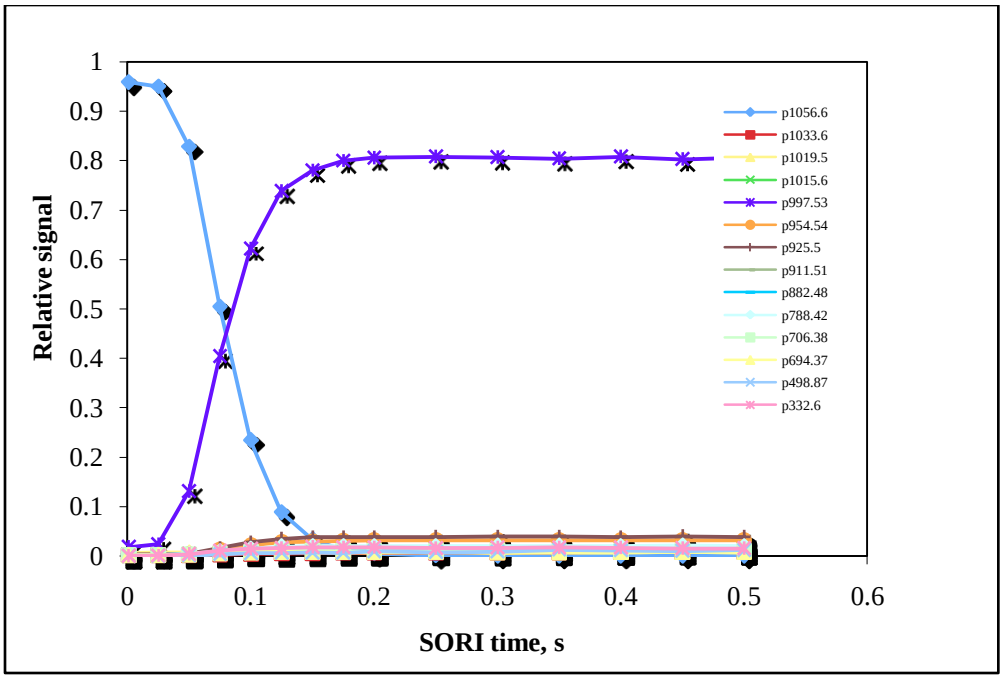

Figure 3.2. Ion yield curves and disappearance curve of $[CH_3(CH_2)_2NH_3@CB6]^+$.

Three general fragmentation pathways can be observed in Figure 3.2. The dissociation channel that most of the $[CH_3(CH_2)_2NH_3@CB6]^+$ ions populate is the loss of neutral propylamine from the complex ion. The ion yield curve of protonated CB6 (m/z 997) represents

this channel. The numerous remaining dissociation products of $[CH_3(CH_2)_2NH_3@CB6]^+$ can be divided into two groups. One is the fragmentation products of the CB6 cage; the other is fragmentation of propylamine, with one fragment remaining bound to CB6. Both of these are minor dissociation channels.

Similarly, these three dissociation pathways can be observed for all of the $[CH_3(CH_2)_nNH_3@CB6]^+$ complex ions (n = 0-8) in the SORI CID experiments. Although the branching ratios among these three pathways for different alkylammonium chains are not the same, the relative abundances of protonated CB6 (around 80%) are always far greater than the relative abundances of the products generated through the two minor channels. This suggests that loss of neutral amine is the lowest energy dissociation channel, which is also in agreement with the result of B3LYP/6-31+G* computational studies.

The observation of CB6 cage fragmentation along with loss of neutral amine suggests that the covalent cleavage of the CB6 cage is competitive with loss of the neutral amine during the dissociation of $[CH_3(CH_2)_nNH_3@CB6]^+$. This in turn suggests that the monoamines are strongly bound to the cage, implying that the alkyl chain of monoamine is included in the CB6 cavity. This is consistent with earlier results for alkyldiamine complexes of CB6, which exhibit even greater cage fragmentation for inclusion complexes, whereas externally bound complexes of alkyldiamines with CB5 fragment exclusively by neutral amine loss.[6] The lowest energy structures found in the MMFF94S conformational search using the Maestro/MacroModel modeling package are also in agreement with internal binding of amine to CB6. Thus we conclude that the monoamine complexes studied here have their alkyl tails included inside CB6 and use the "@" symbol to represent these complexes.

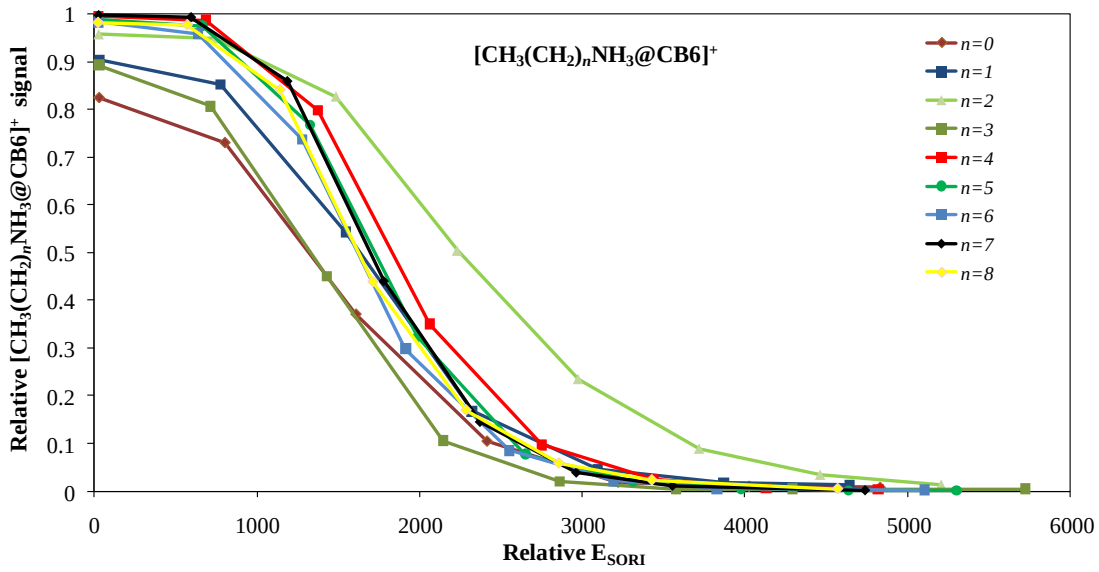

Figure 3.3. SORI disappearance curves for $[CH_3(CH_2)_nNH_3@CB6]^+$ (n = 0-8).

Figure 3.3 shows the disappearance curves for the $[CH_3(CH_2)_nNH_3@CB6]^+$ complexes. The x-axis shows relative SORI energy for the purpose of easy comparison of complexes as n varies. Relative energies for 50% loss of the parent ion, $E_{SORI,50}$, are determined by linear fitting of the falling portion of each disappearance curve and extrapolation to the x-intercept of the fitted line. The energies for 50% loss of the parent ion and standard errors are shown in Figure 3.4. Error bars represent standard errors from the linear fitting procedure used to derive the values.

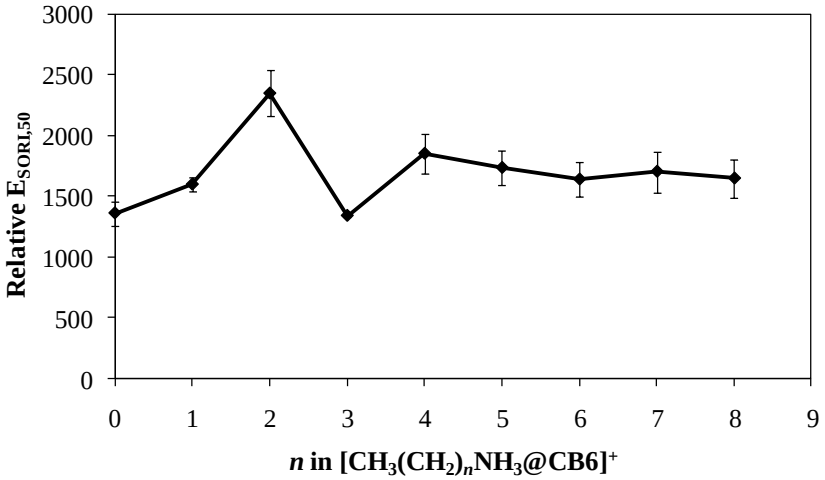

Figure 3.4. Relative SORI energies for 50% loss of $[CH_3(CH_2)_nNH_3@CB6]^+$.

$E_{SORI,50}$ can be taken as an indicator of the overall relative stabilities of the complexes. It reaches a maximum for the $n = 2$ complex in Figure 3.4. In aqueous solution, the maximum binding constant for alkylammonium interacting with CB6 occurs for $n = 3$.[3] For the various monoamines, the ammonium part of the molecule is bound to the CB6 cage and solvated by the CB6. The difference between the various complexes lies only in the lengths of monoamine alkyl tails. In the gas phase, the alkyl tail can be solvated only by the CB6, but in solution it can be solvated either by the ligand or by the bulk solvent. A short tail would be solvated primarily by the CB6 in either gas phase or solution, but additional solvation could occur for a longer tail only in solution. Therefore, it is reasonable that the optimum chain length in the gas phase is smaller than that found in solution.

Binding energies of the $[CH_3(CH_2)_nNH_3@CB6]^+$ complexes can be derived from the computed energies of their components. Experimentally we observe $[CH_3(CH_2)_nNH_3@CB6]^+$ complexes mainly dissociate into singly protonated CB6 and neutral monoamines. Therefore, the

binding energy of $[CH_3(CH_2)_nNH_3@CB6]^+$ complexes, $B(L - M^+)$, can be modeled by calculating the enthalpy change expressed as: $B(L - M^+) = [E(L^+) + E(M)] - E(LM^+)$, where E is the computed energy of each component, L is CB6 and M is monoamine.

N	$[CH_3(CH_2)_nNH_3@CB6]^+$
0	-236.20185
1	-235.38182
2	-231.75196
3	-238.95918
4	-233.71384
5	-232.59853
6	-233.23004
7	-233.33663
8	-233.43781

Table 3.1. Computed energy changes (kJ/mol) for binding neutral monoamine to singly protonated CB6.

The computed binding energies for $[CH_3(CH_2)_nNH_3@CB6]^+$, derived from B3LYP/6-31G* geometry optimizations, are given in Table 3.1. The computed dissociation energies for $[CH_3(CH_2)_nNH_3@CB6]^+$ can be obtained directly from $D(L - M^+) = - B(L - M^+)$. Plotting the computed dissociation energies vs. the alkyl chain length gives Figure 3.5.

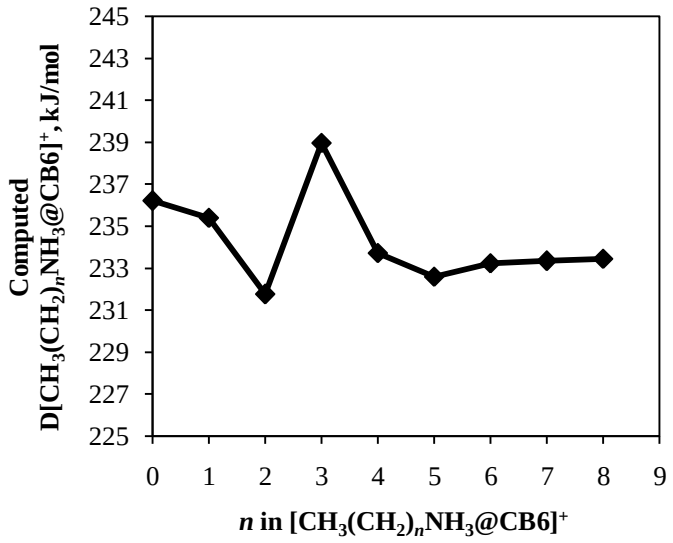

Figure 3.5. Computed dissociation energies for $[CH_3(CH_2)_nNH_3@CB6]^+$.

Comparing experimental (Figure 3.4) with computational (Figure 3.5) dissociation energy trends of $[CH_3(CH_2)_nNH_3@CB6]^+$, we find they both reach a maximum at intermediate size of the ammonium ions and don't change too much when *n* is 4 or greater. In the gas phase, where solvent-release entropic effects are not present, the stabilities and dissociation energies of $[CH_3(CH_2)_nNH_3@CB6]^+$ ions are determined primarily by the hydrogen bond strength between the ammonium ion and the carbonyl dipoles, written as N-H ··O=C. As the alkyl chain length increases, the basicity of ammonium ions increases, leading to stronger hydrogen bonding, but the increase in basicity will be negligible once the chain reaches a certain length. Such effects are apparent in the computational results, but not in the SORI dissociation thresholds. The calculations show increased binding for $n = 0\text{-}2$, with relatively constant binding for $n \geq 4$.

The experiments show the dissociation threshold of $[CH_3(CH_2)_nNH_3@CB6]^+$ is greatest for the $n = 2$ complex, but the computed results suggest that the $n = 3$ complex has the strongest binding. This difference is probably due to the different features of the two approaches in

probing the dissociation energy. The computed dissociation energy is obtained from the energy difference between a fully relaxed complex and fully relaxed products. The experimental threshold data reflects the activation barriers for the dissociation of complex, which will be the same as the computed dissociation energy only when the reaction has no reverse activation barrier. The dissociation of $[CH_3(CH_2)_nNH_3@CB6]^+$ is probably not such a barrier-free reaction. Therefore, the small qualitative disagreement between the computational and experimental results is reasonable.

Reactivity of $[CH_3(CH_2)_nNH_3@CB6]^+$ complex ions was studied on the 9.4 T FTICR mass spectrometer. Singly-charged ions of $[CH_3(CH_2)_nNH_3@CB6]^+$ were isolated, then allowed to react with a pair of neutral amines in the trapping cell. Here the exchange reaction of $CH_3(CH_2)_2NH_2$ for $CH_3(CH_2)_3NH_2$ on $[CH_3(CH_2)_2NH_3@CB6]^+$ is chosen as an example, shown below:

$$[CH_3(CH_2)_2NH_3@CB6]^+ + CH_3(CH_2)_3NH_2 \underset{k_r}{\overset{k_f}{\rightleftharpoons}} [CH_3(CH_2)_3NH_3@CB6]^+ + CH_3(CH_2)_2NH_2 \quad (1)$$

A solution of CB6+$CH_3(CH_2)_2NH_2$ was electrosprayed first for the purpose of reaching equilibrium from the forward direction. $[CH_3(CH_2)_2NH_3@CB6]^+$ ions were isolated and then allowed to react with butylamine for various reaction times. Plotting the relative abundances of reactant ions $[CH_3(CH_2)_2NH_3@CB6]^+$ and product ions $[CH_3(CH_2)_3NH_3@CB6]^+$ vs. reaction time gives the first graph in Figure 3.6. Then the isolation and reaction processes are repeated for electrosprayed $[CH_3(CH_2)_3NH_3@CB6]^+$ ions with the same neutral pressures, so that equilibrium can be reached from the reverse direction. The process is shown as the second graph in Figure 3.6.

In Figure 3.6, the ratio of $[CH_3(CH_2)_2NH_3@CB6]^+$ to $[CH_3(CH_2)_3NH_3@CB6]^+$ finally becomes constant with time within experimental error, and the same ratios are obtained no matter whether the equilibrium is approached from the forward or the reverse direction. Therefore, this reaction has achieved equilibrium. Comparing this reaction with the exchange reaction on $[CH_3(CH_2)_2NH_3•CB5]^+$ in Figure 2.8, the reaction involving $[CH_3(CH_2)_2NH_3@CB6]^+$ takes a much longer time to reach equilibrium. This suggests that $[CH_3(CH_2)_2NH_3@CB6]^+$ is an internally-bound complex since the caged guest is kinetically difficult to displace. This conclusion is consistent with that obtained from its dissociation behavior.

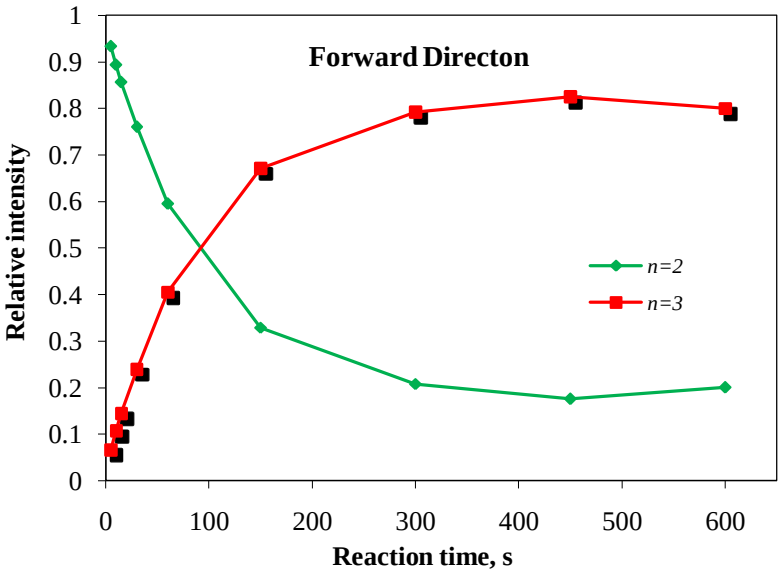

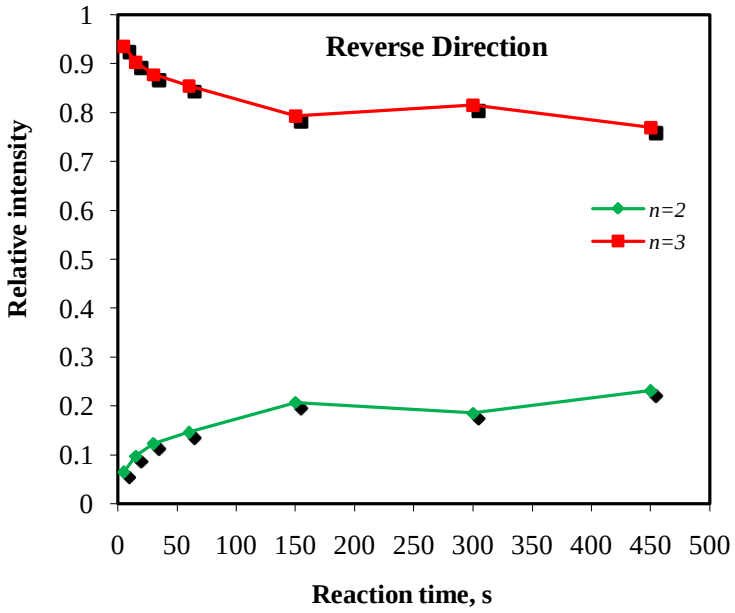

Figure 3.6. Relative abundances of $[CH_3(CH_2)_2NH_3@CB6]^+$ and $[CH_3(CH_2)_2NH_3@CB6]^+$.

Measurement of the equilibrium constant of this reaction was carried out three times each in the forward and reverse direction. The equilibrium constant of reaction (1), K_{23}, was determined using Eqn. (9) in chapter 1 and the results are compiled in Table 3.2. The standard Gibbs free

energy change of reaction (1), ΔG_{23}^{o}, determined using Eqn. (12) in chapter 1, is -8.67 $\pm$0.10 kJ/mol.

Equilibrium constant	1 st	2 nd	3 rd	Average
K_{forward}	30.1	30.5	33.2	32.4 $\pm$1.3
K_{reverse}	32.9	33.0	-	

Table 3.2. Equilibrium constant measured from the forward and reverse directions.

The exchange reactions of primary alkylmonoamines on protonated CB6 were only measured for propylamine (n = 2) through hexylamine (n = 5). The main reason is the exchange reactions on $[CH_3(CH_2)_nNH_3@CB6]^+$ are very slow to reach equilibrium. In order to reach equilibrium, the reactant ions need to be trapped in the ICR cell for a long time, which results in ion loss and weak signal. The other is the $[CH_3(CH_2)_nNH_3@CB6]^+$ complex ions do not give strong enough signal to conduct equilibrium experiments because of the poor solubility of CB6. The standard Gibbs free energy changes as well as the computed energy changes of all these reactions are shown in Figure 3.7. Free energy changes of the reactions on $[CH_3(CH_2)_nNH_3@CB6]^+$ can be obtained by subtracting the free energies of reactants from the energies of products, expressed as:

$$\Delta G_{n,n+1}^{o} = \{\Delta G_{f\,CH_3(CH_2)_nNH_2}^{o} + \Delta G_{f\,[CH_3(CH_2)_{n+1}NH_3@CB6]^+}^{o}\} - \{\Delta G_{f\,CH_3(CH_2)_{n+1}NH_2}^{o} + \Delta G_{f\,[CH_3(CH_2)_nNH_3@CB6]^+}^{o}\}$$

All three reactions have negative ΔG° values. Therefore, it is possible to conclude that $[CH_3(CH_2)_nNH_3@CB6]^+$ complexes become increasingly stable as n increases from 2 to 5. Thus the relative binding affinities of protonated CB6 for primary amines increases in the order propylamine < butylamine < pentylamine < hexylamine.

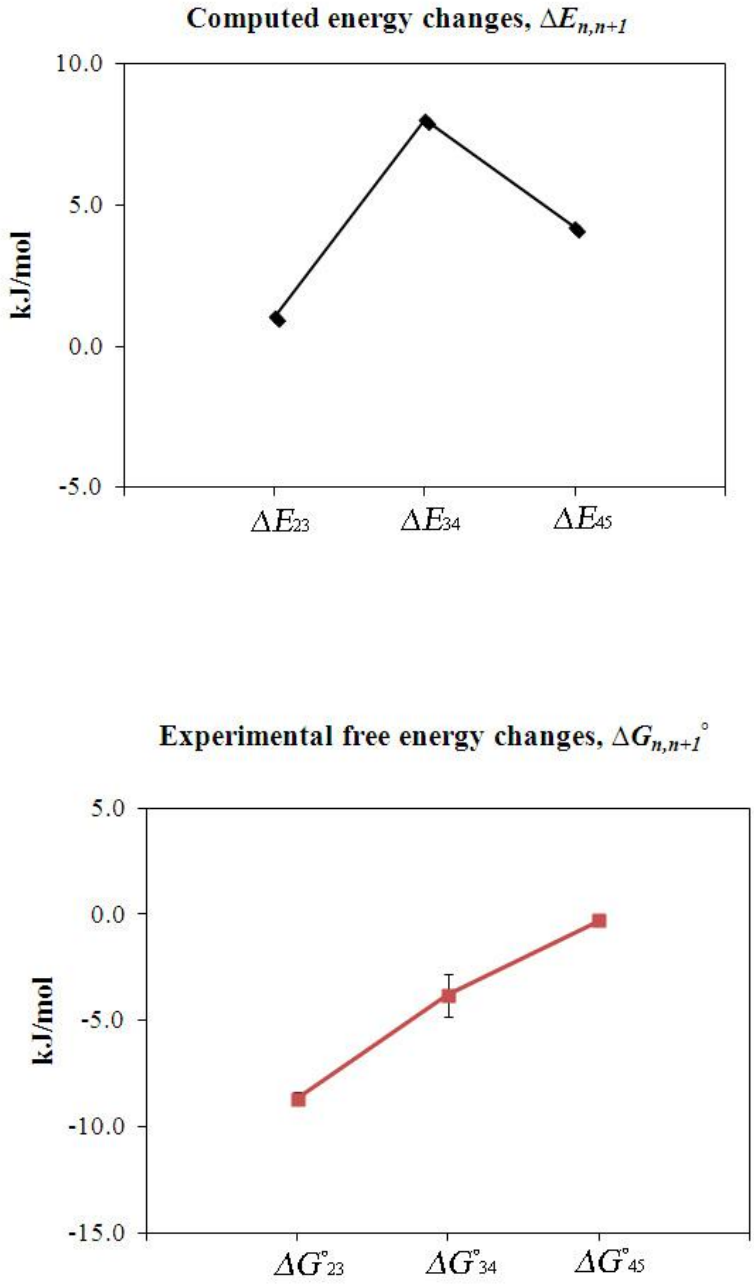

Figure 3.7. Computed energy changes and experimental Gibbs free energy changes and for the exchange reactions on $[CH_3(CH_2)_nNH_3@CB6]^+$.

The experimental values are generally smaller than the computed values, which is the same as Figure 2.12, illustrating the existance of systematic error. As noted above, the CB6 complex ions

undergo very slow exchange process, therefore, they are more easily to be suffered from the pressure drift of gasous neutrals than CB5 and mc5 complex ions. Considering all these possible systematic errors, we can say the experiment and the computed results agree pretty well in the overall trends.

Characterization of CB7 complexes.

The exchange reactions of primary alkylmonoamines on protonated CB7 were only measured for propylamine (n = 2) through pentylamine (n = 4). Figure 3.8 shows the relative abundances of the reactants and products in the exchange reaction of butylamine for pentylamine on protonated CB7.

The rate constants of the exchange reactions on CB7 are generally bigger than those for the corresponding CB5 complexes. The reactions appear to reach a stationary state in just a few seconds. However, the ratio of reactant ions to product ions changes after a longer reaction delay (for instance, 60 seconds). A possible explanation is that both externally-bound and internally-bound structures are present for the CB7 complex. Externally-bound CB7 complex ions would be expected to undergo rapid exchange, whereas we would expect internally-bound CB7 complex ions to react much more slowly. As the reaction time is extended, more and more effective collisions take place between internally-bound CB7 ions and neutral amine molecules. Besides the exchange reaction, an addition reaction also happens. A second butylamine attaches to the 1:1 complex and forms a 2:1 complex. However, this 2:1 complex is not stable with respect to exchange reaction to form the pentylamine complex, so it decays away at longer times. Therefore, the relative abundances of reactants and products will change gradually as the reaction time increases.

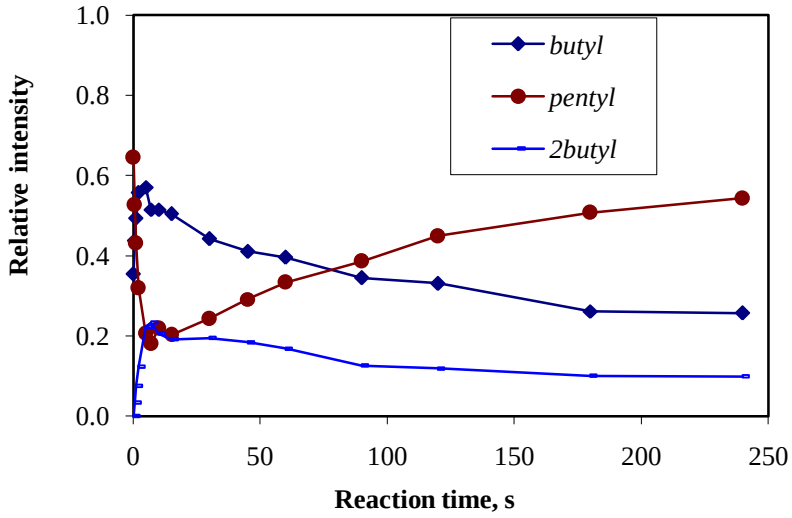

Figure 3.8. Exchange reaction of butylamine for pentylamine on protonated CB7.

Due to the complexity of the reactions on CB7, equilibrium constants and free energy changes of the reactions on CB7 cannot be determined. Besides, the computational methods can only probe the energy changes of the exchange reactions on the internally-bound CB7 complex ions. Therefore, the CB7 experiments are not compared with theoretical calculations here as other cucurbiturils.

Conclusion

Reactivity measurements for the complexes formed by CB6 with alkylmonoammonium ions and observation of their collision-induced fragmentation patterns both confirm the internally-bound conformation of the complexes in the gas phase. Reactivity tests of CB7 complexes exhibit distinctive behaviors which suggest both internally-bound and externally-bound structures are present in CB7 complexes. The dissociation energies for CB6 complexes are

relatively quantified and the highest dissociation threshold occurs for the $n = 2$ complex. The measurement of rate and equilibrium constants provides valuable information on their chemical reactivities. These results suggest that SORI CID and ion molecule reactivity measurements are good methods for probing supramolecule structures for gas-phase ions.

References

(1) Mock, W. L.; Vogtle, F. *Comprehensive Supramolecular Chem.* **1996**, *2*, 477-493.

(2) Lee, J. W.; Samal. S.; Selvapalam, N.; Kim, H.-J.; Kim, K. *Acc. Chem. Res*. **2003**, *36*, 621-630.

(3) Mock, W. L.; Shih, N.-Y. *J. Org. Chem.* **1986,** *51*, 4440-4446.

(4) Kim, K. *Chem. Soc. Rev.* **2002,** *31*, 96-107.

(5) Buschmann, H.-J.; Wego, A.; Schollmeyer, E.; Dopp, D. *Supramolecular Chem.* **2000,** *11*, 225-231.

(6) Zhang, H.; Paulsen, E. S.; Walker, K. A.; Krakowiak, K. E.; Dearden, D. V. *J. Am. Chem. Soc*. **2003**, *125*, 9284-9285.

(7) Dearden, D.V.; Dejsupa, C.; Liang, Y.; Bradshaw, J. S.; Izatt, R. M. *J. Am. Chem. Soc*. **1997**, *119*, 353-359.

(8) Senko, M. W.; Canterbury, J. D.; Guan, S.; Marshall, A. G. *Rapid Commun. Mass Spectrom.* **1996**, *10*, 1839-1844.

(9) Bakhtiar, R.; Holznagel, C. M.; Jacobson, D. B. *Organometallics* **1993**, *12*, 621-623.

(10) Chen, L.; Wang, T.-C. L.; Ricca, T. L.; Marshall, A. G. *Anal. Chem.* **1987**, *59*, 449-454.

(11) Jiao, C. Q.; Ranatunga, D. R. A.; Vaughn, W. E.; Freiser, B. S. *J. Am. Soc. Mass Spectrom.*

1996, *7*, 118-122.

(12) Halgren, T. A. *J. Comput. Chem.* **1996**, *17*, 490-519.

(13) Black, G.; Didier,B.; Feller, D.; Gracio, D.; Hackler, M.; Havre, S.; Jones, D.; Jurrus, E.; Keller, T.; Lansing, C.; Matsumoto, S.; Palmer, B.; Peterson, M.; Schuchardt, K.; Stephan, E.; Taylor, H.; Thomas, G.; Vorpagel, E.; Windus, T.; Winters, C. *Ecce*; Pacific Northwest National Laboratory: Richland, Washington, USA, 2003.

(14) Apra, E. W., T. L.; Straatsma, T. P.; Bylaska, E. J.; de Jong, W.; Hirata, S.; Valiev, M.; Hackler, M. T.; Pollack, L.; Kowalski, K.; Harrison, R. J.; Dupuis, M.; Smith, D. M. A.; Nieplocha, J.; Tipparaju, V.; Krishnan, M.; Auer, A. A.; Brown, E.; Cisneros, G.; Fann, G. I.; Fruchtl, H.; Garza, J.; Hirao, K.; Kendall, R.; Nichols, J. A.; Tsemekhman, K.; Wolinski, K.; Anchell, J.; Bernholdt, D.; Borowski, P.; Clark, T.; Clerc, D.; Dachsel, H.; Deegan, M.; Dyall, K.; Elwood, D.; Glendening, E.; Gutowski, M.; Hess, A.; Jaffe, J.; Johnson, B.; Ju, J.; Kobayashi, R.; Kutteh, R.; Lin, Z.; Littlefield, R.; Long, X.; Meng, B.; Nakajima, T.; Niu, S.; Rosing, M.; Sandrone, G.; Stave, M.; Taylor, H.; Thomas, G.; van Lenthe, J.; Wong, A.; Zhang, Z.; 4.7 ed.; Pacific Northwest National Laboratory: Richland, Washington 99352-0999, USA, 2005.

(15) Chai, Y.; Guo, T.; Jin, C. M.; Haufler, R. E.; Chibante, L. P. F.; Fure, J.; Wang, L. H.; Alford, J. M.; Smalley, R. E. *J. Phys. Chem.* **1991**, *95*, 7564-7568.

Chapter 4

Summary and Perspective

From the experiments presented in this thesis, it has been shown that two versatile tandem mass spectrometry-based techniques, SORI CID (sustained off-resonance irradiation collision induced dissociation) and ion molecule equilibrium measurements, are powerful tools to probe the structures and behaviors of supramolecular ions. However, there are several avenues that can be pursued to gain more valuable insights on the system of cucurbiturils with alkylmonoamines.

Future work on this project would first include doing variable temperature equilibrium measurements of the same systems studied in this thesis. Yongjiang Liang, a previous graduate student of the Dearden research group, obtained the free energy, enthalpy and entropy changes of an exchange reaction on the complex formed by a chiral crown ether host with chiral amine enantiomers.[1] These thermochemical quantities can be acquired by measuring equilibrium constants *K* over a range of temperatures and plotting ln *K* as a function of 1/T, which is a van't Hoff plot. The slope of the resulting line will give us $-\Delta H°/R$ and the intercept will be $\Delta S°/R$.

Another direction with this project could involve the use of the CRAFTI (cross sectional areas by Fourier transform ICR) method to measure the cross sections of the same system studied in this thesis.[2] This measurement will allow us to compare the collision cross sections and see how the alkyl tail influences the binding of the complex.

Other host or guest systems would also be worthwhile to investigate. For example, it would be interesting to replace the cucurbituril with other host species such as α-cyclodextrin and 18-

crown-6 or to replace the alkylmonoamine with diamine and see if similar trends are observed. Finally, valuable information could be obtained by doing theoretical calculations on these systems.

References

(1) Liang, Y.; Bradshaw, J. S.; Dearden, D. V. *J. Phys. Chem. A* **2002**, *106*, 9665-9671.

(2) Dearden, D. V.; Yang, F. *57th ASMS Conference on Mass Spectrometry and Allied Topics*; ASMS: Philadelphia, PA, **2009**.